TECHNICAL ARTICLES
VOL. 01

ASG Superconductors   Leading Superconducting Technology

#fusion

ASG
SUPERCONDUCTORS

This collection of technical articles
by ASG Superconductors from 2018 provides
a vivid illustration of the often complex
activities of a company in the high technology
sector, made possible thanks to the skill
and enthusiasm of all the people who every
day contribute with their work.
Superconductivity was discovered in 1911, but
the technology and applications linked to it are
still "young": recent achievements include the
discovery of the Higgs Boson, the development
and refinement of MRI magnetic resonance
imaging and major steps forward in hadron
therapy. Our current activities promise
to bring us closer to harnessing nuclear fusion,
providing a radical new and inexhaustible
source of energy for the planet.
We can expect many further innovations to
arise from the application of superconducting
technology, which we hope to be able to relate
in future volumes of this collection.

TECHNICAL ARTICLES
VOL. 01

ASG SUPERCONDUCTORS

ITER PFC MANUFACTURING

Six poloidal field coils positioned horizontally around the ITER vacuum vessel and D-shaped toroidal field coils will help with the shape of the plasma and keep it in suspension away from the walls.

ASG is deeply involved in the manufacturing and testing of the poloidal field coils at the Fusion for Energy (F4E) Poloidal Field coils factory, located at the ITER site.

If results of the preliminary tests are positive, the coil is cooled down to a temperature of 80 K, where the following additional tests are performed and/or repeated: pressure drop test and vacuum leak test of the helium circuit, high voltage DC test and current test.

IT'S COLD TEST TIME FOR THE POLOIDAL FIELD COILS OF THE ITER FUSION DEVICE BY THE ASG TEAM!

Alberto Amaduzzi, Eugenio Cavanna, Fabio Fichera, Giulio Pizzigoni (ASG) with the collaboration of Sandro Bonito Oliva, Monica Martinez Lopez (F4E)

Poloidal field coil #6
— the located at the bottom of the ITER machine and the first in line for installation —
has completed all testing on site in the factory of Fusion for Energy. (Courtesy of ITER)

Six poloidal field coils positioned horizontally around the ITER vacuum vessel and D-shaped toroidal field coils will help with the shape of the plasma and keep it in suspension away from the walls. The top poloidal field coil (PF1) will be supplied by Russia; the five lower ring coils are under the procurement responsibility of Fusion for Energy which is the European domestic agency in-charge of the procurement of the European in-kind contribution to ITER. Four of these will be produced on site. (PF6 has been produced by Europe and China.) ASG is involved in the supply of the ITER Poloidal Field Coils PF2, PF3, PF4 and PF5 and the cold testing of PF6, the provision of both the engineering integration services and Project management for the supply of the Poloidal Fields Coils PF2, PF3, PF4 and PF5. This includes definition, description and management of the interfaces between the various contractors participating in the Project.

The Poloidal Field Coils are fundamental components of the ITER experimental fusion device. Together with the toroidal field coils of which we have produced 10 of 19 at our La Spezia workshop, the poloidal field coils shape the plasma and contribute to its stability. Six poloidal field coils are installed in the ITER machine: PF1 to PF6. Four of them, the PF2, PF3, PF4 and PF5 are so large that they have to be manufactured in the ITER site at Cadarache, in France; the remaining two, PF1 and PF6, are comparably smaller and they are manufactured respectively in Russia and in China. The largest coil has a diameter of 24 m, while the heaviest weighs as much as 400 tons. These coils are manufactured using NbTi superconducting cables, due to the lower magnetic field to which they are exposed in comparison with the toroidal field coils which require the higher performing Nb3Sn material. In all cases, supercritical helium is needed in order to reach the operating temperature of both sets of coils. ASG is deeply involved in the manufacturing and testing of the poloidal field coils at the F4E factory, Cadarache. Despite the difficult times due to the covid-19 pandemic, we have not stopped our activities, while taking all safety precautions.
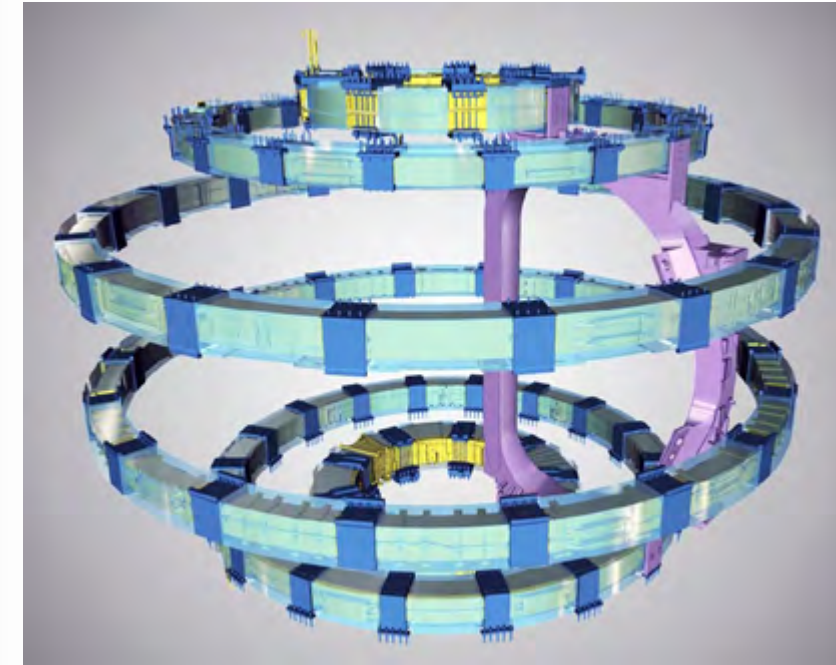

Figure 1 Poloidal field coils of ITER with one toroidal field coil.

Once the manufacturing process is completed, each PF coil undergoes a test campaign inside a cryostat designed and produced for this purpose. While such tests are not performed at the final operating temperature, they nevertheless provide valuable information both to the manufacturing team and to the quality inspectors, and largely increase the general confidence in assembling the tested coils in its final position in the tokamak Initially, before cooldown, a vacuum leak test and a pressure drop test of the helium cooling circuit are performed, together with an electrical DC current test and an electrical insulation (or Paschen) test of the ground insulation at room temperature.
If results of the preliminary tests are positive, the coil is cooled down to a temperature of 80 K, accordingly to the technical specifcation requirements where the following additional tests are performed and/or repeated: pressure drop test and vacuum leak test of the helium circuit, high voltage DC test and current test. Scope of the cold tests is to detect any possible malfunction that may appear after cooldown, that could originate e.g., from the different thermal contraction of materials.
At the end of the tests at low temperature, the coil is warmed up and the previous tests at room temperature are repeated.
All the PF coils will be tested in Cadarache by ASG Superconductors, inside the above-mentioned facility, following the technical specification issued by ASG.
To date, both PF6 and PF5 coils have been fully and successfully tested.

The Cold Test Facility

The Cold Test Facility provides the set of equipment and machinery to perform the cold test of the PF coils at the target temperature of 80K. The facility has been designed to cool down the magnet while minimizing the risk of insulation breakage due to thermal contraction/expansion: for this purpose, the machine is able to decrease the temperature of the magnet with a maximum cooling rate of 1 K/h and can maintain the maximum instantaneous temperature difference between any parts of the coil to less than 50 K at all times during the cool-down and warm-up phases.

The Cold Test Facility (CTF) is composed of two main systems: the cryogenic plant and three cryostats to host the different size of the PF coils.

The cryogenic plant creates the pressurized cold helium gas flow that will circulate through the PF coils. The 80 K temperature regime is reached by passing helium gas through a heat exchanger in direct contact with liquid nitrogen at 77 K.

The cryogenic plant is also able to supervise the cooldown and acquire additional information by interfacing with auxiliary devices installed on both the cryostat and on the PF coil during the whole thermal cycle. An acquisition system monitors the data of temperatures, pressures, flows, etc..; a video recording system of 40 vacuum video-cameras monitors the coil under Paschen conditions; a leak detector performs leak testing of the coil at room and cold temperature and a power supply and electronics are used to measure the coil resistance by applying an electrical current of 500 A at low temperature.

The cryostats are stainless-steel vacuum chambers designed to host the coil and to reduce thermal losses during the test by conduction, convection and radiation. To mitigate these effects, the chambers employ thermal shields, superinsulation material, fiberglass supports and provide a vacuum level of 10^-5 mbar.

From a geometrical point of view, the dimensions of the cryostats have been determined by the size of the different PF coils, their diameter ranging from 12 m for the smallest PFs to 27 m for the largest ones Each cryostat is designed to withstand the coil weight (up to nearly 400 tons) and it is constructed out of modules of stainless-steel. The modules are joined together and welded, creating the complete donut-shape vacuum chamber that contains the coil during the tests.

Figure 2 The dedicated area for the cryostats: On the right, the smaller cryostat is assembled and cold testing of the PF6 coil is in progress. On the left, the medium sized cryostat is about to be assembled for the final cold test of PF5.

Cool down of the coils

As explained in the previous section, through the CTF we control the cooling rate and the temperature gradient along the coil. The coil is instrumented with Cernox and Pt100 thermometers and the electrical resistance of each double pancake is measured and converted into an average value of temperature.

The coils are cooled by a flow of He gas that is circulating along the cooling circuit of the coil, by means of temporary piping that connects the inlet and outlet of the coil to the valve box.

Two other circuits, in parallel with the main one, provide the He gas for cooling down the coil clamps and the thermal shield of the cryostat.
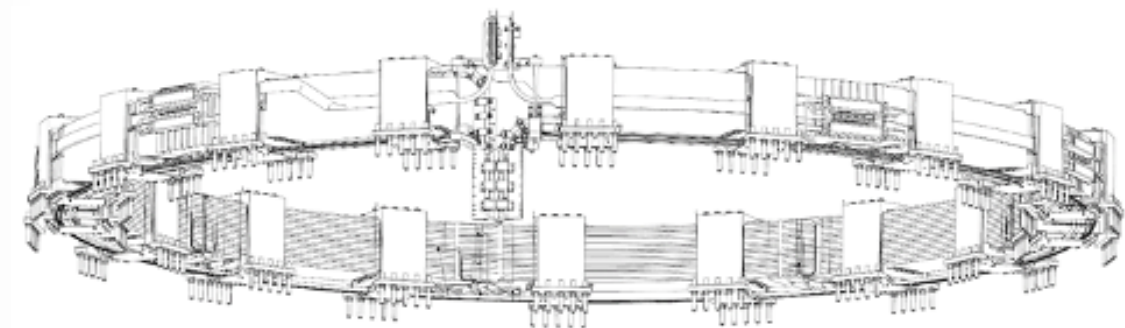

Figure 3 PF5 isometric view.

The cooldown is controlled by the mass flow of helium which circulates in the circuits, and the nominal cooling rate stays between 0.8 and 1 K/h. Thus, for a cooldown of a coil to 80 K, about 13 days are needed, including an initial transient time and time for the final stabilization of the temperature.
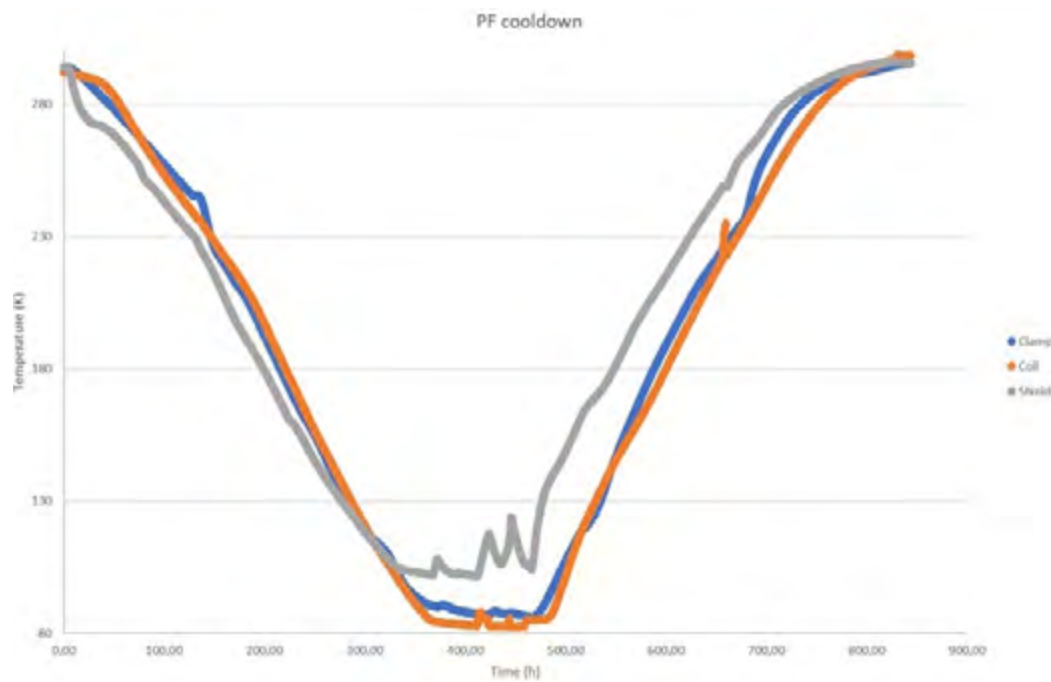

Figure 4 Cooldown and warm up of PF6.

At the end of the tests at cold temperature, the coil is warmed up again controlled by the flow of He gas.

Tests performed on the PF coils

Several tests are performed on each coil. The following tests are carried out at room temperature before and after the cooldown: pressure drop test, leak test, high voltage DC test and Paschen test.
The following tests are performed at 80K: pressure drop test, leak test, high voltage DC test and current test.

Pressure drop test

The pressure drop test confirms the performance of the hydraulic circuit that is used to refrigerate the coil at cryogenic temperatures. Any leak, bottleneck, or increased friction against the cold helium flow would result in an increase in pressure drop. As the pressure drop is compensated by the cooling system, it cannot exceed certain values otherwise the coil will not be able to maintain the appropriate operating temperature.
In this experiment, a dry helium gas mass flow (g/s), which is circulated in the coil by a compressor, is set at different values so that the flow rate can be correlated to the difference between the measured inlet and outlet pressures (pressure drop). Indeed, the magnet offers a hydraulic impedance, an "opposition" to the helium flow and the higher the gas mass flow, the higher the pressure loss that will arise. This test is performed controlling the helium gas mass flow and monitoring the pressure of the gas which enters and exits the magnet through dedicated pipes. It is successfully passed when the results are compliant with research studies that can be found in literature, along with the results of previous tests performed on ITER superconducting magnets.
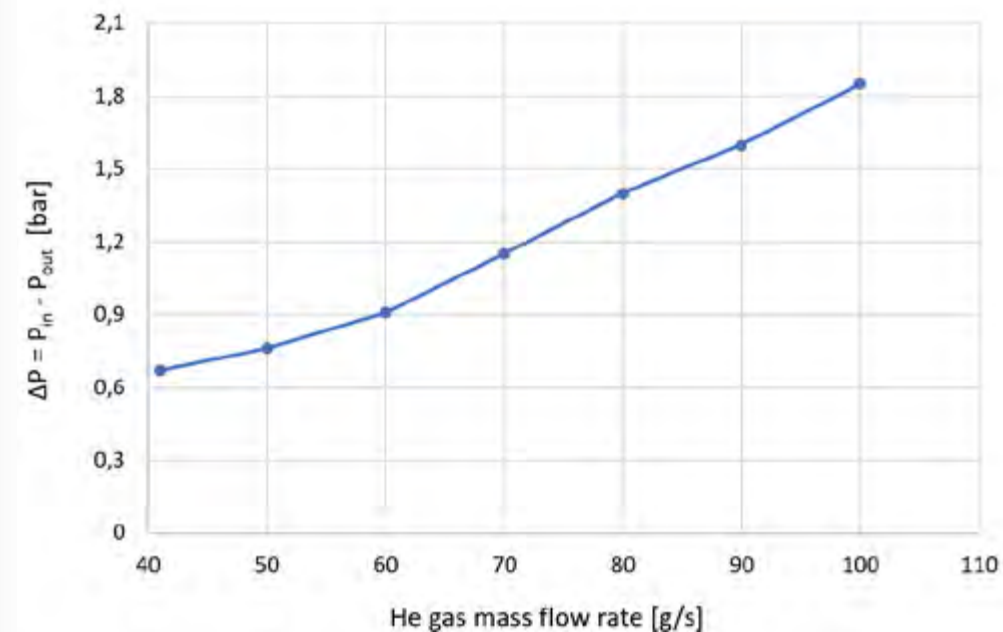

Figure 5 Pressure drop test on PF6 after cool-down at 80 K.

High voltage DC test
When the current in a superconducting magnet is ramping up and down, and in an unlikely case of a quench, a voltage appears on the superconducting coil. A high voltage DC test is therefore required to be sure that no significant leakage current appears through the electrical insulation material.

In this experiment, a maximum voltage of 15 kV is applied across the magnet, reaching this value after a ramp of about 17 V/s, and is held constant for 5 minutes. The test is passed if the insulation resistance at 15 kV is higher or at least equal to 500 MΩ, which corresponds to a leakage current lower than 30 µA.

Leak test
The cooling process down to cryogenic temperature can produce considerable thermal stresses which can cause the formation of leaks. Therefore, it is necessary to perform a leak test before and after this process. First of all, the helium flow rate in the magnet is set to zero and its pressure is set to 15 bar. The leak rate measured at this pressure is then recorded by means of a helium leak detector which is connected to the cryostat. Given a certain volume, the helium leak rate provides a measurement of the change of pressure over time, due to the flow of some amount of the noble gas. Should a leak be present, helium would flow out of the magnet and its circuit and into the cryostat and would be measured by the leak detector.

Then, a calibrated leak into the cryostat is opened in order to check if a leak of known magnitude can be detected and correctly measured. Subsequently, the calibrated leak is closed and the helium inside the coil is pressurized at 30 bar. After waiting for one hour in this configuration, the leak rate is measured again, and then the calibrated leak is opened. The helium leak rate measured at 15 bar is then subtracted from the rate at 30 bar and if the result is lower than 10^{-6} mbar*l/s the test is passed successfully.
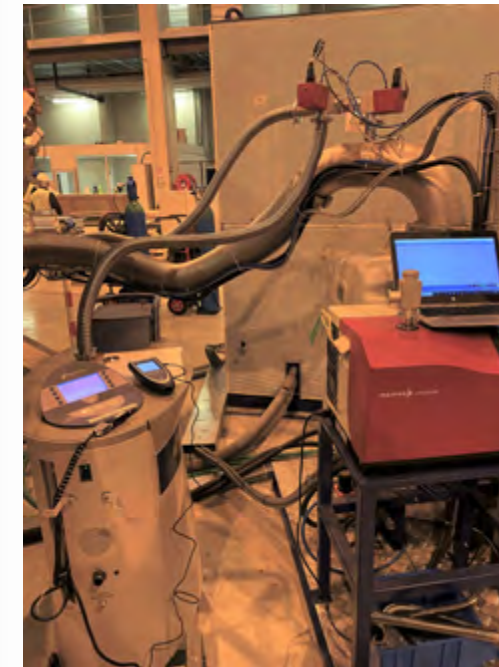

Figure 6 Leak detector, on left side, and vacuum pumping system connected to PF5 cryostat.

Current test
The current test is undertaken to ascertain the homogeneity of the electromagnetic architecture of the superconducting coil.

This test, performed only at low temperature, consists of feeding the coil with 500 A and recording, from the voltage taps that are installed on the coil, the voltage drops across each double pancake. The voltage drop across a shunt resistor is also measured in order to calculate the actual current flow in the coil. All these signals are then acquired using a fast acquisition measurement device at a sample rate of around 100k sample/s. The results are analysed and the test is considered successful if the modulus of the difference between the resistances of each double pancake is lower than 5%.

Paschen Test
In order to minimize the probability of an electrical breakdown at operating voltage, for example in case of an accidental pressure-rise, the electrical equipment has to be Paschen-tight, meaning that no breakdown may occur across a range of pressures. Figure 7 shows the heavy dependance of the breakdown voltages of various gases on the product of the gas pressure and the distance between two electrodes at different electric potential.

The Paschen test is performed at room temperature before and after cooldown.
A DC high voltage is applied to the coil at different levels of nitrogen gas pressure from 10-2 mbar to 100 mbar in the cryostat. At each pressure step, a voltage of 15 kV is applied for 1 minute. An electrical breakdown would cause an increase in the leakage current, detected by the high voltage generator and a flash, hopefully located by the cameras in the cryostat. The criteria for passing the test are having a leakage current lower than 20 μA and not observing any discharge.
Once this last test is passed after the cooldown and warm-up, the cold testing of the coil is completed and the magnet is ready for the final operations before being delivered to ITER for assembly in the tokamak.
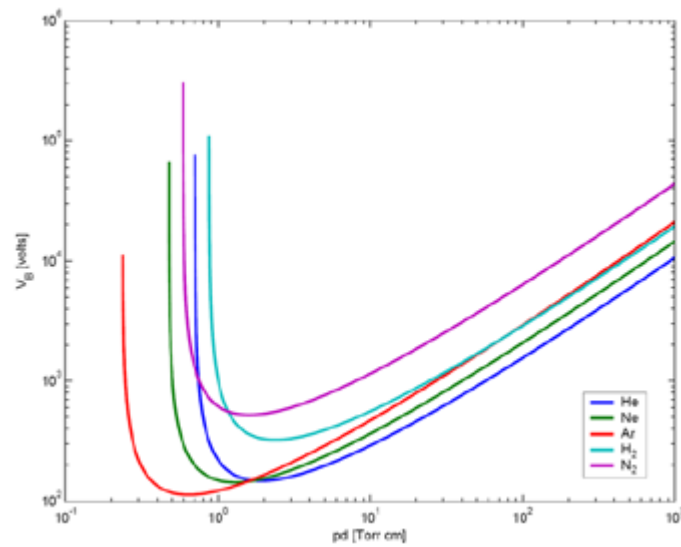
Conclusions
The poloidal field coil cold test represents an exciting moment for the ASG team to verify that the lengthy manufacturing work of the huge superconducting systems was carried out successfully.
The cold tests on the PF6 confirmed the integrity of the coil, which passed all the tests carried out. The tests performed so far on the PF5 have also been successfully passed. The Cold Test Facility operated correctly during all the phases of the activity, with no noteworthy problems. The activities have been supervised 24 hours a day by the ASG team, both on-site and remotely, with support from Fusion for Energy and other personnel.
This activity was made possible by a remarkable effort of coordination and teamwork between different entities from all around the world with a common goal: to build the ITER device.

Figure 7 Paschen curves for different gases. He and N2 plots are relevant f
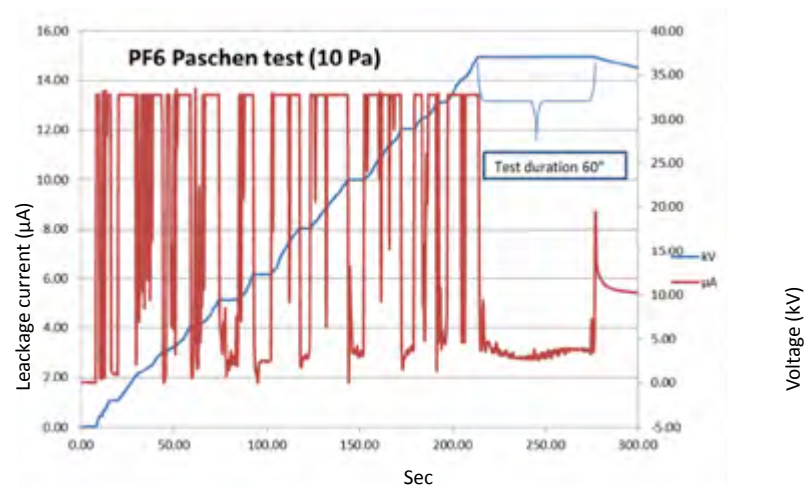or the tests on ITER superconducting magnets.

Figure 8 : Paschen tests on PF6.

JT-60SA TOROIDAL FIELD COILS

The assembly of the tokamak was completed in 2020 and at the end of the same year also the cooldown was executed; on 02/03/2021 the complete toroidal system was fed up to the nominal current of 25.7 KA.
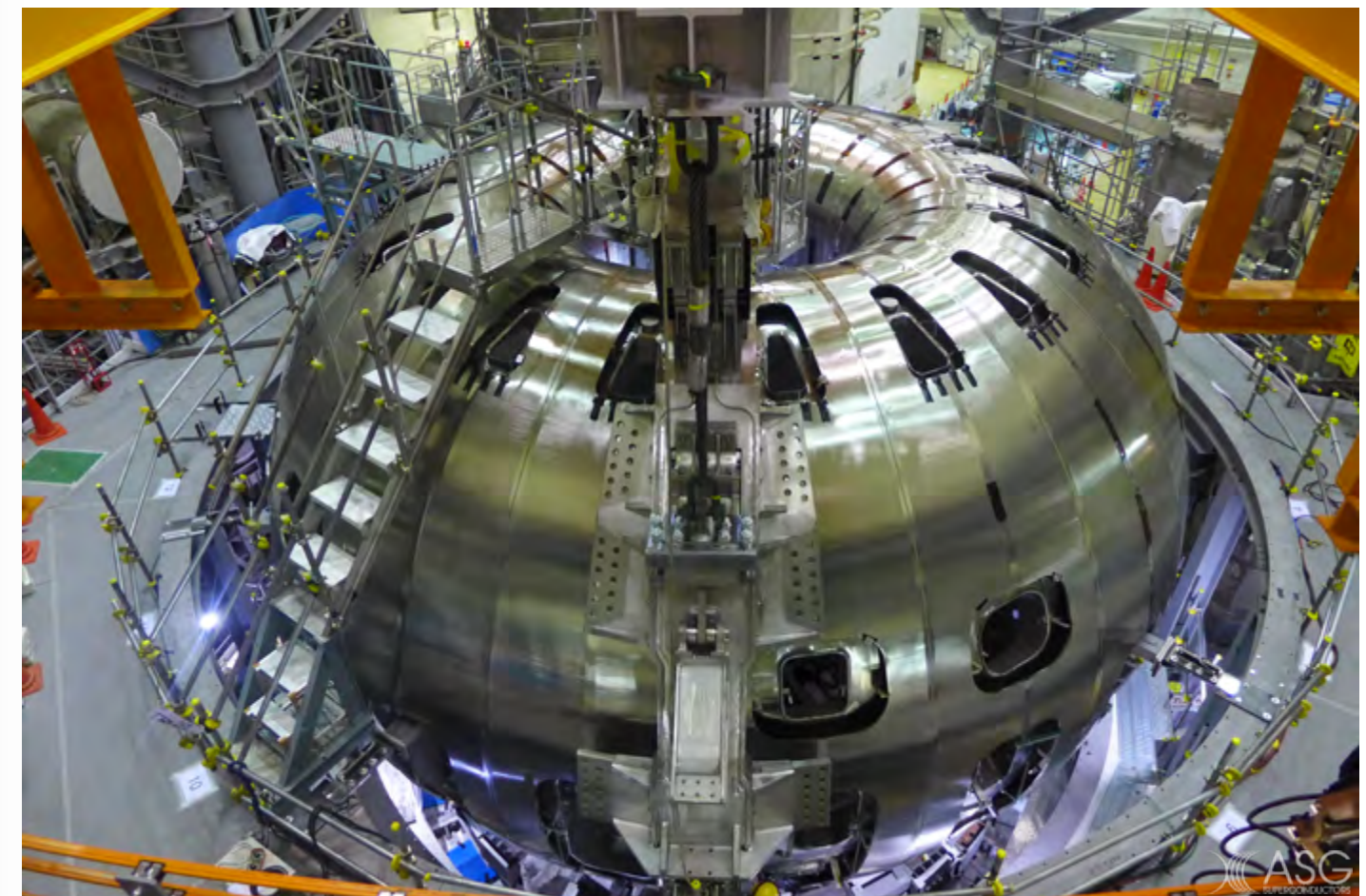
JT-60SA is a superconducting tokamak machine designed to contribute to the early realization of fusion energy by supporting the exploitation of ITER and research toward DEMO by addressing key physics issues, installed at Naka site in Japan.

The Italian Atomic Energy Agency ENEA awarded the contract for the manufacture of 10 Toroidal Field Coils (9+1 spare) for the JT-60SA project to ASG Superconductors.

JT-60SA TOROIDAL FIELD COILS (TFC) MANUFACTURE

Giovanni Drago

Insertion of the last coils
in the machine (Courtesy of JAEA)

Introduction

In 2011 under the framework of the Broader Approach Agreement between the European Atomic Energy Community and the Government of Japan, the Italian Atomic Energy Agency ENEA awarded the contract for the manufacture of 10 Toroidal Field Coils (9+1 spare) for the JT-60SA project to ASG Superconductors. The manufacture of the remaining 10 TF coils necessary for the project was managed by the French Atomic Energy Authority.

The superconducting tokamak machine at the Naka site in Japan is designed to contribute to the early realization of fusion energy by supporting the exploitation of ITER and research toward DEMO by addressing key physics issues.

To achieve this, JT-60SA is designed to be completely superconducting and thus able to produce 100 s long shots with a plasma current IP of about 5.5 MA.

The toroidal magnetic system is composed of eighteen D-shaped coils, wound using NbTi conductor, capable of generating a maximum field of 2.25 T on the central axis of the plasma and a maximum field of 5.65 T at the innermost equatorial plane of the coil straight leg. The modules are operated at a temperature of 4.4 K with a theoretical temperature margin of 1 K. They are energised by a current of 25.7 kA.

Coil description

Each coil is manufactured starting from a CIC (Cable in Conduit conductor consisting of a Cu-NbTi strands rope (strand diameter Ø=0.81 mm) wrapped with a thin stainless-steel band and inserted in an AISI 316L stainless steel jacket 2 mm thick. The overall conductor dimensions are 22.0 × 26.0 mm with a void fraction of 32%.

Figure 1, 2, 3 Details of the JT-60SA conductor

The conductor is wound in D-shaped Double Pancakes (DP) consisting of two layers of 6 turns each, insulated by means of two wrappings of half-overlapped fiberglass tape.

After winding, 6 DPs are stacked together to form the Winding Pack (WP) of each coil. The WP cross-section dimensions are 150 × 347 mm with overall width of ~5 m and length of ~8.2 m including the electrical joints between DPs and terminations.

Once the WP has been assembled and ground insulated using fiberglass tape, it is impregnated with epoxy resin inside a vacuum tight case assembled and welded all around the winding.

Then the WP is inserted into a thick stainless-steel casing able to contain all the magnetic forces acting on the conductor during operation. The total weight of the coil is ~16 tons.

Process qualification and manufacturing tooling procurement
During the first year of the project activities were focused on the following three different tasks:

    a) Definition of the detailed manufacturing plan and preparation of detail drawings of the relevant components.
    b) Conceptual design and development of the tooling for the WP and TFC manufacturing.
    c) Preparation of samples and mock-up for the validation of the design and process qualification to verify that the envisaged procedure meets the main design requirements.

Design Validation

The most important process to be qualified is the turns insulation, consisting of fiberglass tape impregnated with epoxy resin, required to meet stringent requirements in terms of shear strength derived from the calculated mechanical forces acting between the turns.
The performance of the insulation in terms of ultimate shear strength and capability to withstand the cyclic loading has been evaluated on standard samples, comprising two stainless-steel plates separated by fiberglass epoxy resin, simulating the inter-turn insulation. The sample were tested both at room temperature and at 4 K as well as under fatigue conditions and were shown to meet the following requirements:

    — minimum shear strength capacity after impregnation of 55 MPa at 4 K, corresponding to 40 MPa at 300 K
    — minimum shear strength capacity after 36,000 cycles of 20 MPa at 300 K

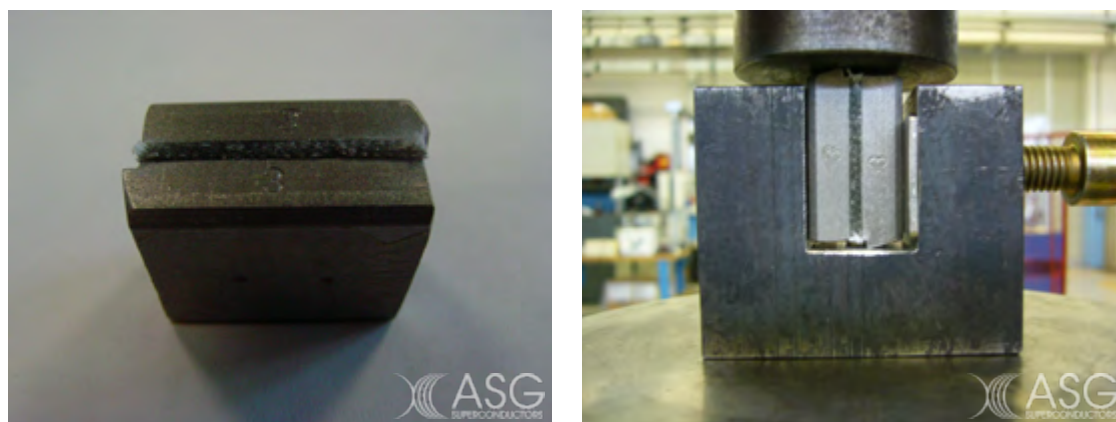The following show the shear strength sample under test:

Figure 4, 5 Shear Test Sample / Shear test sample during testing

The insulation and impregnation processes were also validated by the manufacture of a 1 m impregnation beam, using straight stainless steel bars to represent the WP cross section. The beam was assembled, insulated and VPI impregnated and then submitted to electrical test to verify that all the requirements for the insulation were satisfied. The ground insulation was successfully tested up to 15 kV, while the turns insulation reached 10 kV. In both cases, no faults were detected. The following show the impregnation beam already painted with conductive varnish for grounding:
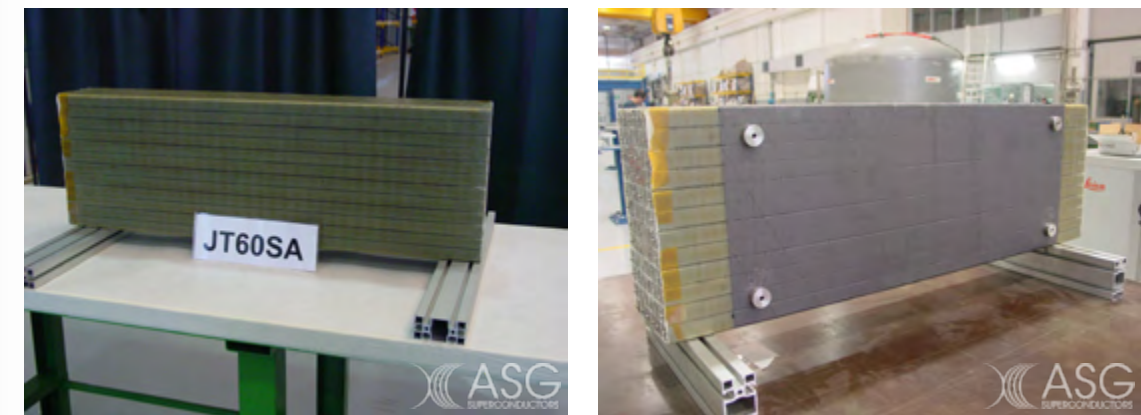

Figure 6, 7 Impregnation Beam / Impregnation Beam with grounding paint and reference markers

The impregnation beam was used also for the qualification of other processes: as a first step it was instrumented with thermocouples and inserted into the coil casing mock-up to verify that the temperature increase during the casing welding was not high enough to damage the resin of the impregnated WP.
Then, after welding, the mock-up was submitted to a second impregnation cycle in order to simulate the embedding impregnation. The mock-up cut after the impregnation is shown in the following images:

Figure 8, 9 Impregnation Beam inside casing mock-up / Casing mock-up cut after embedding impregnation

Another important process to be qualified was the manufacture of the internal joints which provide the electrical junction between different DPs of the coil. The joints are realized following the "praying hands" concept based on the configuration where the two conductors forming the joint are coming from the same side of the coil. The conductors are inserted into a pre-machined junction box made from a three-layer (stainless steel – copper – stainless steel) explosion bonded plate, pressed against the low resistance copper intermediate plate and compressed by the stainless-steel covers which are welded to the main body of the box. The electrical resistance of the joint at 4 K had to be less than 5 nΩ. To guarantee the low resistance of the joint, silvering of the inner surface of the box as well as the end portion of the conductor rope is necessary and several trials and mock-ups were required to define the silvering process parameters. The joint sample shown in the following figure was tested by ENEA with positive results:

Figure 10 Full size joint sample tested by ENEA

Manufacturing tooling

In parallel with the mock-ups and process qualification work, the conceptual design of the main tooling was performed followed by the procurement and installation of the main tooling for the manufacture of the coils. The most critical item was the winding line which is composed of different units assembled and synchronized to perform the DP winding. In detail the line is equipped with an unwinding spool which supplies the conductor necessary for the winding, a straightening unit to remove any residual bending present on the conductor, a cleaning unit, a calendaring unit to bend the conductor to the required radii, a sandblasting unit, a taping unit and finally a winding table which hosts the bent conductor.

The unwinding spool and the winding table are shown below:

Figure 11, 12 Winding Line-Unwinding spool / Winding Line-Winding Table

Another important tool necessary for manufacturing the WPs is the impregnation station which consists of a steel framework equipped with several modules able to allow the thermal expansion of the WP during the impregnation cycle. The framework can be tilted along the longitudinal side to ease the resin flow during impregnation. Each module is equipped with frames to transfer to the WP the force to compact the insulation and with heating elements to regulate the temperature of the coil during the process.

Figure 13 Impregnation station

The integration of the WP inside the casing required the design of a specific tool able to support the WP during the assembly of the casing parts and to tilt the final assembly to a vertical position in which to perform the casing welding to achieve annular containment of the whole surface of the WP. A challenging aspect of the design of this tool was the small gap between the WP and the casing, being only 5 mm, which strongly influenced the design of the WP supports. The dimensions and loads of the tilting toll required verification of the floor capacity.

Figure 14 Assembly and tilting tool

Manufacturing plan
The Toroidal Field Coil (TFC) manufacturing was divided into two steps – one for each of the main components supplied by ENEA: the conductor for the winding and the stainless-steel casing for the final assembly of the coil. At the end of each manufacturing step, a complete acceptance test was performed.

WP manufacturing
The first step is the WP manufacturing which starts with the conductor acceptance test to assess the conductor tightness. The conductor supplied as a single layer solenoid was inserted into the vacuum chamber to perform the pressure/leak test, evacuating the chamber and pressurizing the conductor. All the conductor lengths tested showed a leak rate lower than 2×10^{-9} mbar*l/s as required by the specification. After the test, the conductor is transferred to the winding line for the DP winding operations: the conductor is first straightened to remove the previous bending deformations, then it passes through the cleaning unit to clean the jacket surface by means of detergent and ultrasound bath.

The next equipment of the line is the bending unit which, by means of plastic deformation, gives to the conductor the required curvature radii for the DP. Once the conductor is bent, the sandblasting unit gives to the conductor surface the roughness necessary to ensure good adhesion of the insulation (fiberglass and resin). This unit represented the most challenging set up, due to the need to operate on a low curvature radius of the turns in the transition region from the straight part to the outer region of the coil. The next unit is the taping machine which applies to the sandblasted conductor the fiberglass tape to realize the turn insulation. Finally, the wound turns are transferred to the winding table.

Figure 15, 16 DP winding completed / Winding of DP 2nd layer

Once the winding operations have been completed the DP is moved by means of the lifting tool to the DP insulation station where several operations are completed: bending the DP leads, removing the jacket and silvering the superconducting rope for the next joints, and applying the DP insulation.

The completed DP is then moved to the stacking station where six DPs forming the WP are stacked together; in this phase, checking and adjustment of the alignment is performed. After stacking, the ground insulation is manually applied by wrapping the WP with several tapings up to the final thickness of 3 mm. A further check on shape and dimensions is performed prior to moving the WP to the impregnation station. The requirements in terms of tolerances were quite demanding especially in terms of the overall dimensions of the WP: on the cross-section of the coil the tolerances are ±3 mm on the width and ±5 mm on the height and referred to the coil dimensions (4370 × 7330 mm) these represent 0.04 & 0.06 %. In addition, the most stringent requirement is set on the centerline of the WP straight part which has to stay inside a cylinder of Ø2 mm.

Figure 17 DP stacking

After application of the ground insulation the WP is moved to the impregnation station where it is inserted inside the impregnation mold which consists of a thin stainless-steel casing split into two halves which are welded all around the WP to realize the resin containment. During this operation the shape of the WP is checked by means of the Laser Tracker to control the alignment within the prescribed tolerances. Moreover, after the welding and prior to starting the process cycle, the tightness of the casing is verified to ensure that the the maximum leak rate is not exceeded. The ground insulation of the WP is checked and the mold is used as a vacuum vessel to check the leak rate on the conductor and internal joints/terminations.

Once the mold has been checked, the VPI impregnation cycle can be executed performing all the different phases controlling the temperature vs. time as well as all the other parameters. The whole impregnation cycle, including the preliminary heating, the ramping up and down to the different temperatures and the final cool down to room temperature (RT) lasts about 12 days.

After the VPI cycle the WP impregnation casing is dismantled and the WP is cleaned before the application of the conductive varnish to realize the electrical grounding.

Figure 18, 19 WP VPI impregnated / WP after grounding varnish application

On the completed WP the intermediate acceptance tests are performed, executing a complete dimensional survey and referring the results, especially the centerline position, to the reference points (12 in total) glued on the inner surface of the WP. These reference points are used for the next assembly operation and for the final interface machining.

In addition, hydraulic tests on the conductor circuit are performed inside a dedicated vacuum chamber: pressure/leak test is performed by pressurizing the conductor up to 30 bar and measuring the leak rate with respect to the chamber, then a flow test is carried out to verify that during the impregnation no obstruction of the conductor circuit occurred. While the WP is inside the vacuum chamber, Paschen tests comprising consisting of High Voltage tests in a gas atmosphere at different vacuum/pressure conditions are also performed. These are executed in N2 gas at different pressure steps from vacuum (10-3 mbar) to 100 mbar. At each step a voltage of 3.8 kV is applied to the conductor to test the electrical tightness of the insulation.

Finally, the standard electrical test (inter-turn and ground insulation) and measurements (Resistance and Inductance) are executed.

This test campaign releases the WP for the next manufacturing stages.

Figure 20 WP introduction into Vacuum chamber for testing

TFC manufacturing

The second step is the TFC manufacturing which starts with the insertion of the WP inside the stainless-steel casing which consists of two main "C" shaped parts 50 mm thick to be assembled and welded to provide containment around the outer surface of the WP. The inner closure is ensured by 20 mm covers that have later to be welded to the "C" shaped parts. For the insertion of the WP inside the casing, only a small clearance is provided: this small 5 mm gap requires that the dimensions and tolerances both of the WP and the casing are well respected to allow the assembly. Due to the precision achievable on the WP following resin impregnation being lower than the precision of the casing components obtained by mechanical machining, the gap is not constant all around the WP surface. For this reason a fiberglass cloth to be further impregnated has been chosen as the filling material, the thickness of which was determined by means of a full geometrical survey both of the coil and the casing. Firstly, the two parts of the casing are installed on the carriages while the WP is positioned on the inner core of the tilting tool. Secondly, the assembly of all the components is performed. Finally the assembly is tilted into a vertical position to allow the execution of the welding between the two parts of the casing. Once the transversal welding has been completed, the coil is tilted again into a horizontal position and moved onto supports for the installation and welding of the inner covers.

Figure 21, 22 WP and coil casing onto the assembly tooling / Assembly tilted in vertical position for welding execution

Figure 23 Cover welding

After the casing welding, the coil is ready for the embedding impregnation of the fiberglass in between the WP and the casing to secure the WP position with respect to the casing. For this VPI impregnation the casing acts as a mold ensuring the tightness for the resin injection and only the blanking of some openings, for example the reference point on the inner surface, is necessary.

A complete dimensional survey follows the embedding impregnation to define the reference planes to be used for the final interface machining. These reference planes are defined by the position of the centerline of the straight leg and are characterized with respect to the reference point of the WP. During the machining other references on the outer surface of the coil are added to allow the final installation. The final machining operations have been commissioned to an external company which performed the activity under ASG responsibility and supervision.

Figure 24 TFC interface machining (courtesy of Officine CLP)

After machining the coils were returned to the ASG premises for completion, comprising the routing, welding and insulation of the cooling circuit as well as the installation and routing of instrumentation. Once the coil has been completed all the acceptance tests were performed and attended by ENEA and the leak/pressure test was also attended by a certified third party.

Figure 25 TFC completed

Coil testing and installation

All the JT60-SA TF coils were successfully tested at the CEA site (near Paris). The test was carried out at cold condition feeding each coil up to the full current of 25.7 kA, including an induced quench obtained by reducing the LHe flow. After the testing, before the shipment to Japan, the OIS (Outer Interface Structure) which represents the mechanical interface between two adjacent coils inside the machine was assembled. Both the testing and OIS assembling activities were in charge to Fusion For Energy. Performed under responsibility and supervision of the European Agency for Fusion (F4E-Fusion for Energy)

The assembly of the tokamak was completed in 2020 and at the end of the same year also the cooldown was executed; on 02/03/2021 the complete toroidal system was fed up to the nominal current of 25.7 KA.
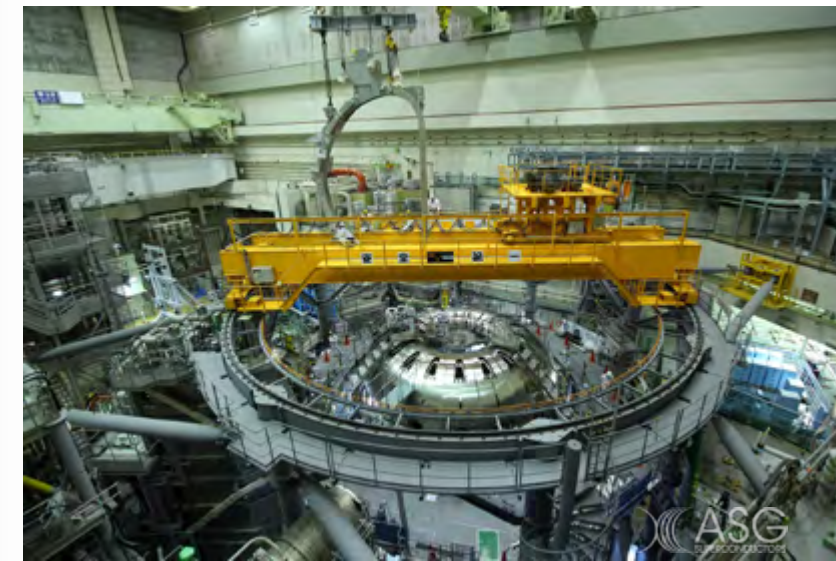

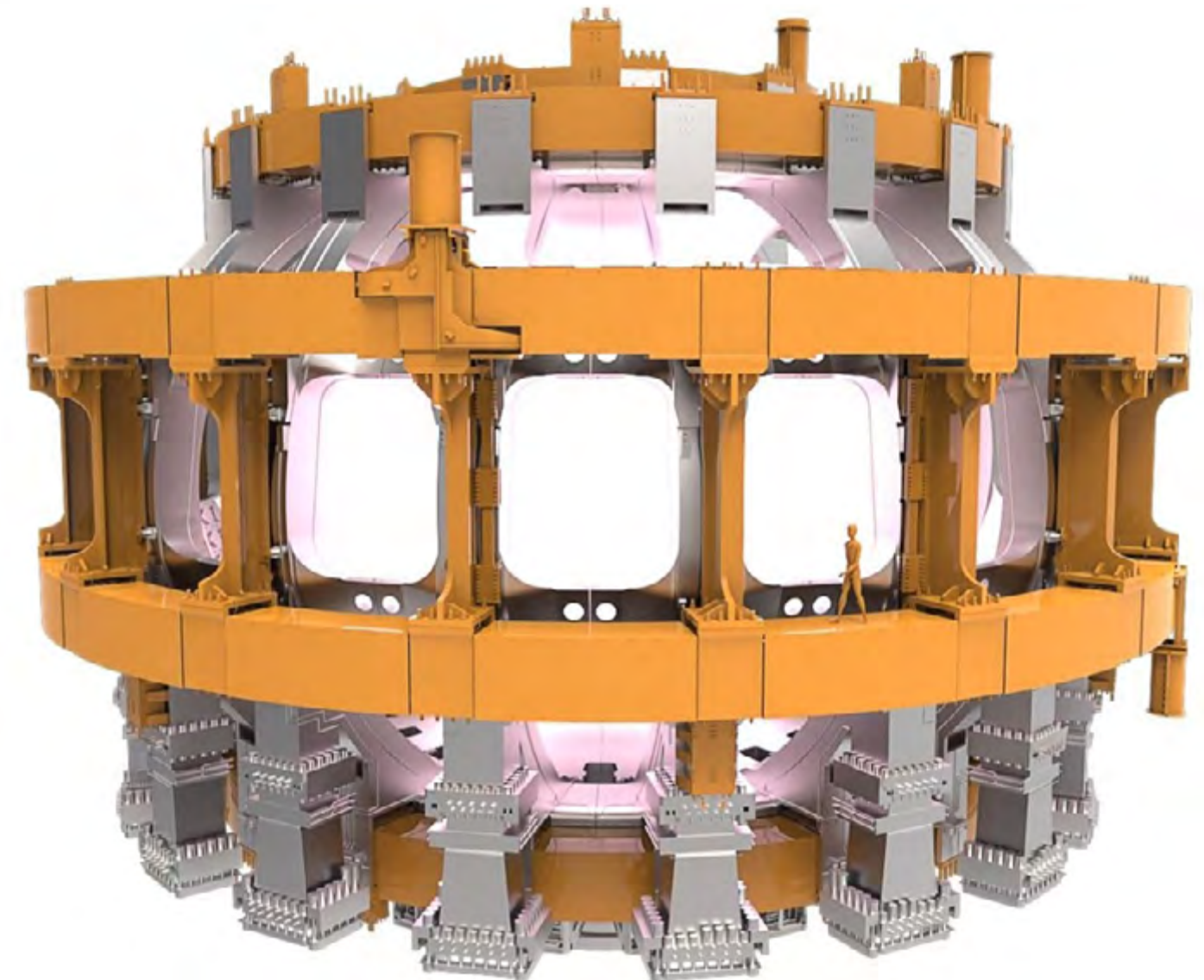**Figure 26** TFC assembling on the machine (Courtesy of JAEA)

ITER PF6
COLD TEST

PF6 COLD TESTED AT TEMPERATURES SIMILAR TO PLUTO

All pictures courtesy of ITER

In the coming months ASG Superconductors will celebrate several important milestones for the production of the poloidal field coils that will be part of the biggest fusion device - ITER.
Seven parties are building the biggest Tokamak machine to test fusion energy through magnetic confinement.
This experiment will allow scientists to study a "burning plasma" that will produce a greater thermal output (500 MW).
Due to their large sizes, i.e. 17 and 24 m diametre, four of the six PF coils are manufactured on-site (Cadarache), in a dedicated workshop under the supervision of Fusion For Energy. Once ready they will be handed over to ITER Organization for their assembly.
The PF coils will be positioned horizontally around the ITER vacuum vessel, and the 18 D-shaped toroidal field coils, to control the shape and stability of the plasma.

At the end of January, the sixth poloidal field coil left the factory and was put into storage until assembly. It was manufactured jointly by F4E and ASIPP (China). Then, it was cold-tested at 80 K by ASG and F4E. A temperature similar to Pluto - the furthest and smallest planet in our Solar system.
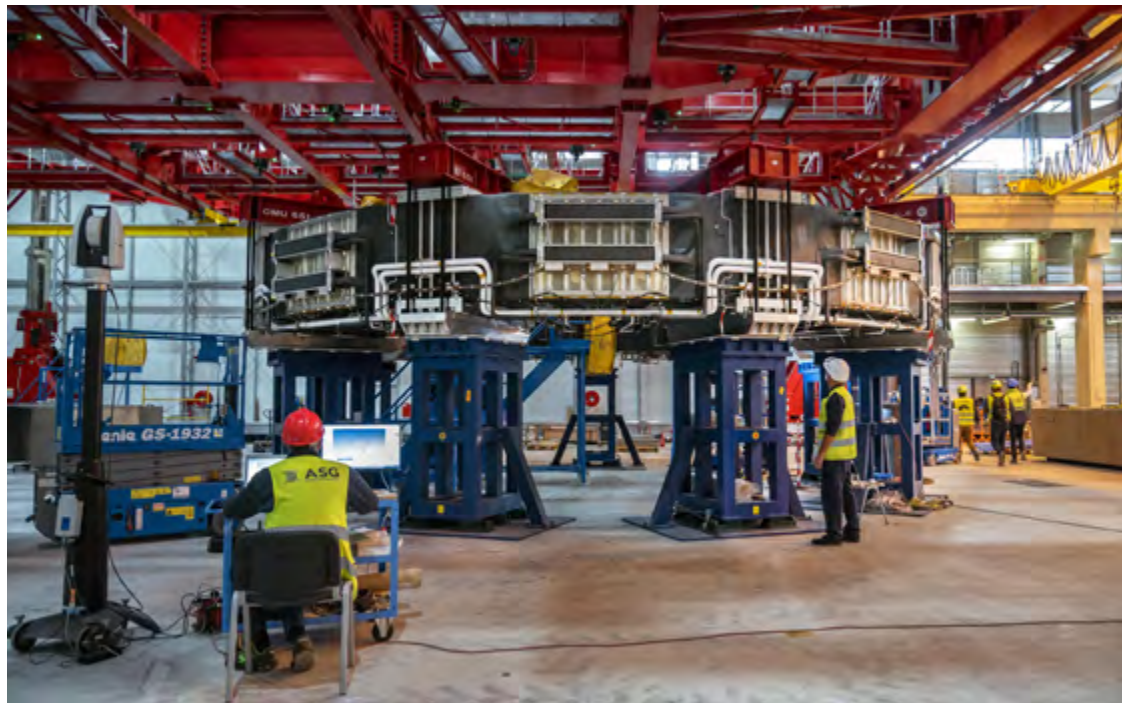
In April, the fifth poloidal field coil will be completed. It's the first to be entirely manufactured on-site.
The first part of its production has been performed by CNIM following ASG Superconductors manufacturing procedures and drawings, constantly under our and F4E's supervision.

The insertion into the tokamak pit of the sixth and fifth coils, will pave the way for an important ITER milestone: the start of TF (Toroidal Field) coil assembly inside the Tokamak building, where the machine will be housed.

This year the second poloidal field coil will be delivered.
Its diameter is around 17 m.
In the meantime, the fourth poloidal field coil is in progress, with a diameter of around 24 m.

Together with Fusion for Energy and the other companies, we continue to work every day for fusion energy.
We will keep you informed on the progress of the biggest international partnership that will bring the power of the Sun to Earth.

#ITER #magnets #pfcoils #tokamak #coldtest #f4e #manufacturing #innovation #fusionenergy

MAGNETIC FLUX DENSITY

Merging metrology with magnetic measurement: developing innovative and cost effective solutions for a flexible field mapper.
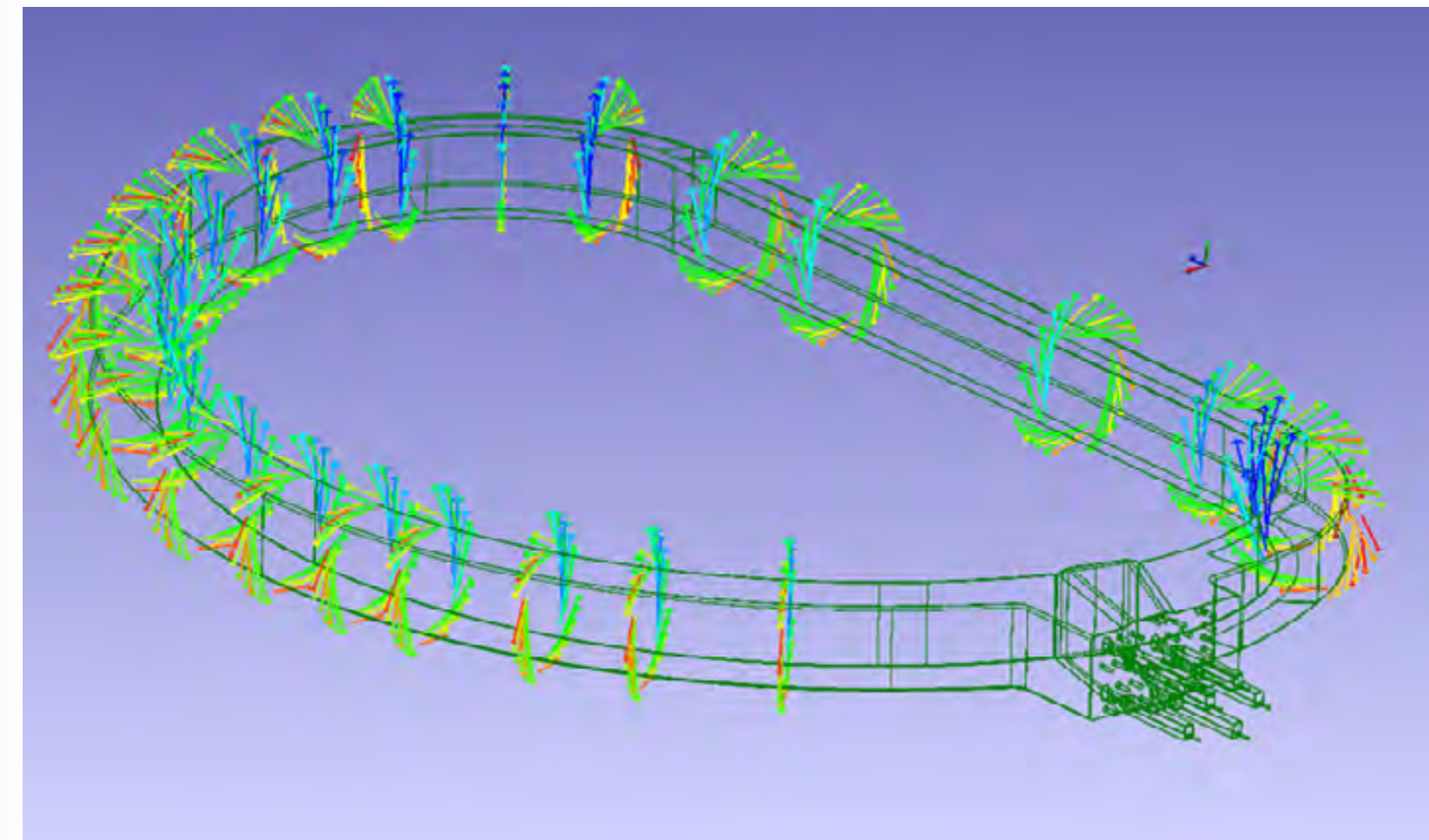
In magnet fabrication technology the effective magnetic field is the final indicator of the quality of the job.

Commercial solution are not flexible enough to cover all the needs of the workshop by using only one device.

This paper describes a flexible and innovative tool for the magnetic field mapping for the following case study: ITER Toroidal Field Coil Winding Pack WP magnetic flux density measurement.

HIGH PRECISION MAGNETIC FLUX DENSITY MEASUREMENT

Alberto Barutti, Matteo Bargiacchi

Merging metrology with magnetic measurement: developing innovative and cost effective solutions.

When ASG started the engineering of the ITER contract and the development of the necessary fabrication technology it started as well to face a very challenging technological goal: how to obtain very large component with high accuracies. Fusion for Energy (F4E), our customer, asked for the definition of some indicators for the as-built performances,
after the coil manufacturing, to check that the product quality fulfils the requirements and to allow the integration inside the reactor of the components supplied by ASG with the others produced by other firms.

The most important key indicators in the definition of our coils as-built performances were identified to be:
— the as built dimensions
— the insulation system performances
— the room temperature magnetic field fingerprint. This is an indicator that allows to understand the quality of the internal geometry of the coils without accessing to the internal part of the coil.

Once the WP is completed it is not possible to access the internal components; the final assembly on the reactor must be driven by using a combination of the results of the test campaign during fabrication and after completion.

Cold tests campaign, that could allow to reach a field big enough to make easy measurements with large accuracies, is too expensive and not included in our scope of supply. Therefore, we decided to design a tool in order to guarantee enough accuracy to make the reconstruction of the magnetic field around the coil possible, by solving an inverse problem, with a very low field. This was useful also because at room temperature it's not possible to feed the coils with high current to avoid heating and large component deformations.

https://fusionforenergy.europa.eu/

A first step was the Design of Experiment, whose results were the main parameters for the test design:
— Requirements of the workshop area.
— Huge number of points to be measured.
— Position and field measurements accuracy.
— Maximum current on the coil (i.e. maximum field available) in order to avoid thermal deformations.

The tool should have been robust, industrial, within time and budget: no ready commercial solution was available.

— **Goal**: obtaining a map of the magnetic field around the coil at standard temperature
— **Delighter**: speed and flexibility of the measurement system
— **To solve**:
    → No commercial solution available.
    → Required accuracy is close to the best available technology.
    → We are an industry, not a laboratory.
    → Very low magnetic field: approximately 150 G (15mT). As a comparison, the earth magnetic field is approximately 1000 times smaller (0.5G = 50µT) and the peak field of the magnet is 1000 times bigger (118 000 G = 11.8 T).
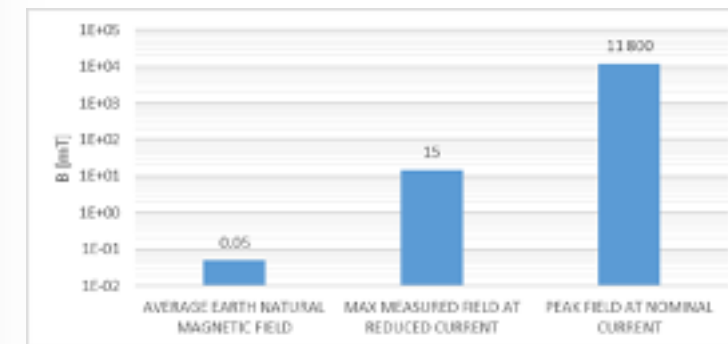

Figure 1. Magnetic field ranges in logarithmic scale.

Only after a long scouting some custom solutions was found, but they seemed too difficult to be developed in a timely manner, not robust enough and with poor flexibility. In the scouting process we understood that a flexible solution should be preferred, both for the scope of the project and for future transfer to other applications.

A flexible field mapper, in fact, is needed for environmental field mapping, including the fringe field on the installations, the fringe MRI field mapping and many other uses. In particular, such technology is useful where it is necessary to sample a big number of measured points in a short time, with no predetermined location in space but with a precise knowledge of their position (it will be shown that it is possible to get points with a precise positioning).
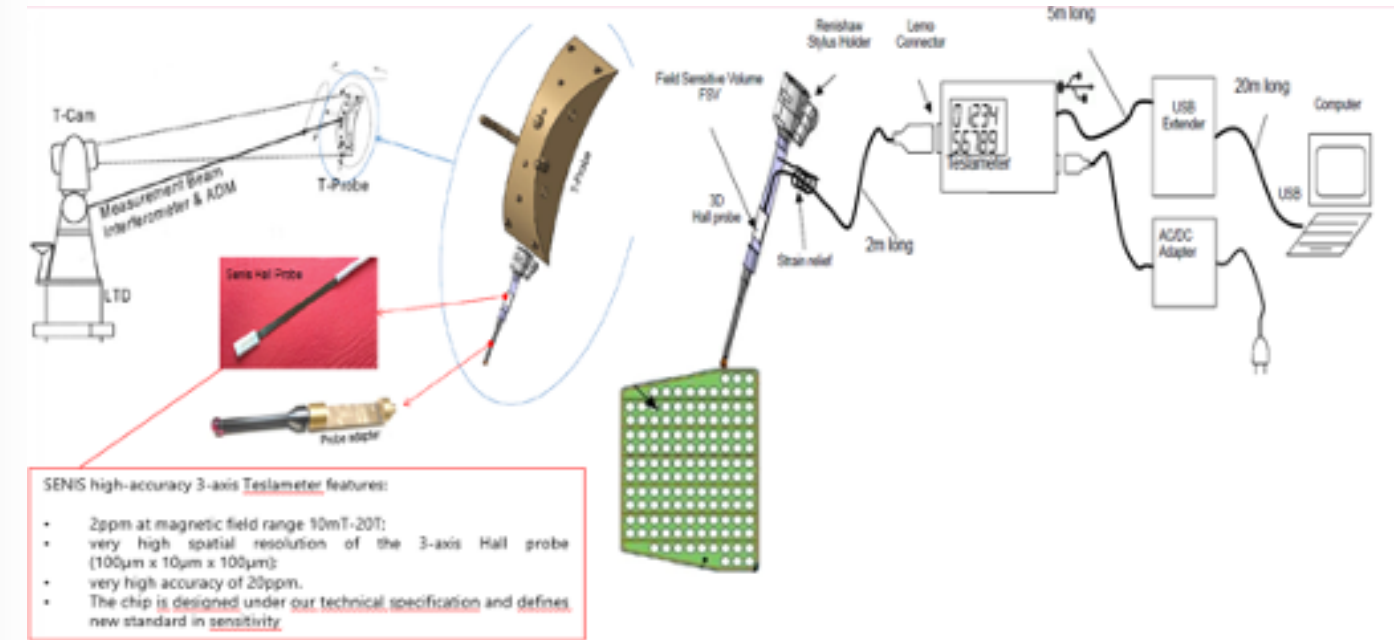
All these reasons convinced us to turn to an internal solution, by adapting the technology and know-how already in our possession.

So, we started to implement our solution, based on the merging of two supposedly distant worlds, metrology and magnetic measurements, which turned out to be an innovative measurement system based on a laser tracker and a Hall probe.

The main advantages of this configuration are:

— The possibility to share the same reference system between metrologic and magnetic measurements (and correlating results).
— The flexibility to measure objects with virtually all shapes and dimensions (no theoretical limit to dimension).
— It is possible to map a large volume of space obtaining the three components of the magnetic field and the position of the probe immediately with one measurement.
— Thanks to the innovative design of the hall probe (with a very small sensible volume) it is possible to operate in highly inhomogeneous magnetic fields without significant loss of information.
For a smarter use of this system, we developed a software plugin that allows to measure the magnetic field directly through the GUI (Graphic User Interface) of the commercial metrological software that we have adopted for the laser tracker management, making it easier to use the tooling and the generation of the output.

SENIS high-accuracy 3-axis Teslameter features:

- 2ppm at magnetic field range 10mT-20T;
- very high spatial resolution of the 3-axis Hall probe (100μm x 10μm x 100μm);
- very high accuracy of 20ppm.
- The chip is designed under our technical specification and defines new standard in sensitivity

1. Introduction and scope of the measurement campaign within the ITER project

[1] https://www.iter.org/mach/magnets

Regarding the ITER TF project, each of the 18 Toroidal Field Coils Winding Packs (TFC-WPs) is composed of 134 turns made of niobium-tin (Nb_3Sn), generating a peak field of 11.8T and storing 41GJ[1]. Fabrication and assembly tolerances might generate sensible deviations from the expected nominal field generated inside the Tokamak.

The magnetic Flux Density Field $\vec{B}$ generated by the TF coil is therefore characterized through the definition of the Current Center Line (CCL) of each TFC-WP. The CCL is defined as the *single turn* that best approximates the field generated by the complete winding of each single TFC-WP, i.e. the solution of the inverse problem that minimizes the difference between the measured and nominal values of the magnetic field $\| B_M - B_N \|$, and represents the fingerprint of each coil. Current specifications for the ITER project require the reconstruction of the 3D position of the CCL for each TFC-WP, for the purpose of using these data during the final alignment of the coil inside the Tokamak. In order to achieve such a goal, it is essential to measure the field produced by the TFC-WP, at room temperature, with a tight accuracy.

2. The instrumentation concept, calibration and uncertainty essentials

A fully integrated 3-axis Type C hall probe[2] has been designed and realized in order to map the 3D field generated by the TFC-WP. Hall Effect is a well-known principle widely used for a broad range of applications, from proximity sensors in their simplest forms, to magnetometers. Hall Effects is based on the Lorentz force that electric charge carriers experience while travelling in a conductor immersed in a transverse magnetic field B. The displacement of the charges within the sensor generates an electric field mutually perpendicular to the current I and B. The hall probe sensible volume HSV measures 0.1 × 0.1 × 0.1 mm: it is embedded into an outer volume of about 8 x 4 x 0.9mm3 and mounted on the stylus of a Leica T-probe[3] as shown in Figure 3. The Leica T-Probe is a 6 Degrees of Freedom PCM device (Portable Coordinate Measurement) based on the combination of photogrammetry and an Absolute Laser Interferometer (AIFM). A T-probe simultaneously measures the position and the orientation of the device. Such a feature is essential to characterize the HSV with respect to the absolute reference frame of the object under measure.
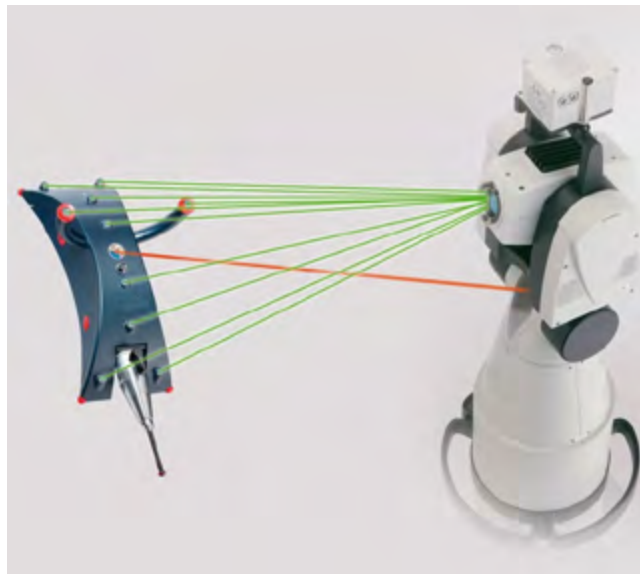
[2] https://www.senis.ch/magnetometer/hall-probes

[3] https://www.hexagonmi.com/it-IT/products/laser-tracker-systems/leica-probing-solutions/leica-tprobe

HALL SENSOR

Figure 3. ASG integration of a SENIS Type C Hall Probe inside the stylus of a Leica T-Probe. The white cable connected to the electronics supplies the DC current to the sensor and measures the DC voltage generated by the Lorentz force. A reference frame is defined centered on the T-Probe.

Figure 2. Leica Laser Tracker 6 DOF system (T-Probe). The position of the reflector is measured via the AIFM (red beam). The orientation of the device is measured via the T-Cam and a set of LEDs embedded on the surface of the target device (green beams).

Figure 4. A picture shot during the R&D activities in 2016 on a WP, before its ground insulation.

This device concept requires a careful calibration activity. In practice, a set of matrix transformations is necessary to retrieve the real magnetic field from the raw magnetic field measured by the Teslameter and the 6 DOF measured by the T-Probe. This was the main activity carried out during the last months of 2016 and the first half of 2017 up to the first successful measure of the magnetic field generated by a WP, performed in June 2017. The accuracy with which the transformations matrices are calculated greatly influences the accuracy of the final measure. The calibration activity determines the final uncertainty of the measure and is the core of the present work.

The absolute field defined with respect to the absolute reference frame TGCS (Tokamak General Coordinate System, see Figure 12, later in this paper) of the object under analysis is $\vec{B}_{TGCS}$. This is the final output, starting from the raw field vector $\vec{B}_{H}$ that the operator can to read on the screen of the Teslameter. Anyway, the Teslameter does not know the orientation of the 3 axis of the HSV with respect to the absolute reference frame. Two transformation matrices $\underline{R}$ and $\underline{C}$ must be applied to the vector $\vec{B}_{H}$. Matrix $\underline{R}$ is a pure roto-translation (orthogonal matrix) coming from the Euler angles of the T-probe stylus R_x, R_y and R_z and absolute position $\vec{r}$. It requires no additional calibration and varies in each measure, according to the orientation of the T-probe with respect to the absolute reference frame. Matrix $\underline{C}$, on the other hand, is a non-orthogonal matrix resulting from calculation, and constant for all the measures.

The calibration of the system is embedded in matrix $\underline{C}$. The raw field vector $\vec{B}_{H}$ is roto-translated according to the Leica angles R_x, R_y and R_z and absolute coordinates vector $\vec{r}$ to obtain the field referred to the absolute system $\vec{B}_{TGCS}$. The expression is:

$$\vec{B}_{TGCS} = \underline{R} \cdot \underline{C} \cdot \vec{B}_{H} = \underline{R} \cdot \vec{B}_{T\text{-}Probe}$$

It is straightforward to understand that the so called calibration matrix $\underline{C}$ is a function of the orientation of the hall axes with respect to the T-probe axes. Its definition is:

$$\underline{C}^{-1} = \begin{bmatrix} \vec{x}_H^{\,T} \\ \vec{y}_H^{\,T} \\ \vec{z}_H^{\,T} \end{bmatrix}$$

Each line of matrix $\underline{C}$ is the transposed vector representation of each hall axis in the reference frame of the T-probe (see Figure 3).
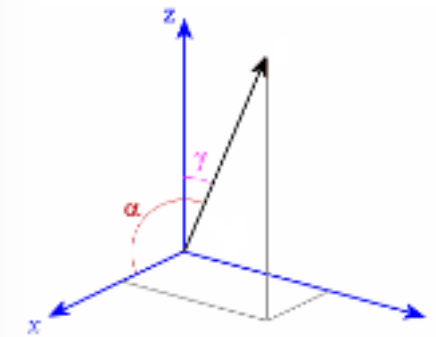

Figure 5. Vector representation of a single Hall probe axis inside the xyz T-probe reference frame (r = 1). Frame in figure is the same shown in Figure 3.

Actually, the chain of measure requires a careful calibration at different level to minimize the uncertainty related to the measure. Low level calibration and temperature corrections is provided directly by SENIS, the probe supplier, via firmware integration. This will be included in the uncertainty model but is not the object of this paper or of additional evaluations. We will see that its contribution to the final uncertainty will be automatically included during the calibration process. Geometrical calibration, synthetized in the constant calibration matrix $\underline{C}$, is essential to compensate for the following assembling imperfections:

    1. Non orthogonality of the hall probe's axes $\mathcal{H}$**no**
    2. Misalignment of the hall probe's orthogonalized axes $\mathcal{H}$**o** with respect to the orthogonal T-Probe axes $\mathcal{T}$

Variable	Symbol	Correction applied	Application level
Voltage output	$\vec{U}_{RAW}$	—	Firmware
Corrected voltage output	$\vec{U}_T = \vec{U}_T(\vec{U}_{RAW})$	Temperature compensation	
Raw field	$\vec{B}_H = \vec{B}_H(\vec{U}_T)$	Standard calibration curve from -40mT to 40mT per each component	
Orthogonalized Field aligned to T-Probe relative reference frame	$\vec{B}_{T-Probe} = \underline{C} \cdot \vec{B}_H$	Sensitivity evaluation with respect to 3 orthogonal axes + Orthogonal rotation with respect to relative (T-probe) axes	Constant calibration matrix applied in the software $\underline{C}$
Field aligned to absolute reference frame	$\vec{B}_{TGCS} = \underline{R} \cdot \vec{B}_{T-Probe}$	Roto-translation	Variable transformation matrix $\underline{R}$ applied at each measured point

Calibration and uncertainty evaluation were at first performed in collaboration with the Italian National Institute for Metrologic Research (INRIM[4]) in 2017. INRIM supplied a calibrated Helmholtz Coil[5] that was used to produce a steady and uniform reference field in the measurement range (see Figure 6). The reference field is aligned to the X axis of the HH coil and its homogeneity ΔH / H is smaller than 1e-4 in a sphere of 10 mm radius. This feature allows to place the HSV inside a homogeneity volume that is big enough to assume that the field measured is always the same in the absolute reference frame of the HH coil aligned to the Laser Tracker.

[4] https://www.inrim.it/

[5] F. Fiorillo, G.F. Durin, L. Rocchino,
A reference system for the measurement of low-strength magnetic flux density,
Journal of Magnetism and Magnetic Materials, Volume 304, Issue 2, 2006.

Essentially, the HH Coil from INRIM was used to calculate the calibration matrix $\underline{C}$. The hypothesis is that the reference field $\vec{B}_{REF}$ inside the homogeneity volume is constant regardless the position and orientation $\underline{R}_i$ of the sensible volume. The raw data from the 3 axis of the sensor $\vec{B}_{Hi}$ and the matrix $\underline{R}$ are registered and an GRG optimization loop is deployed to calculate the best coefficient of the calibration matrix $\underline{C}$.
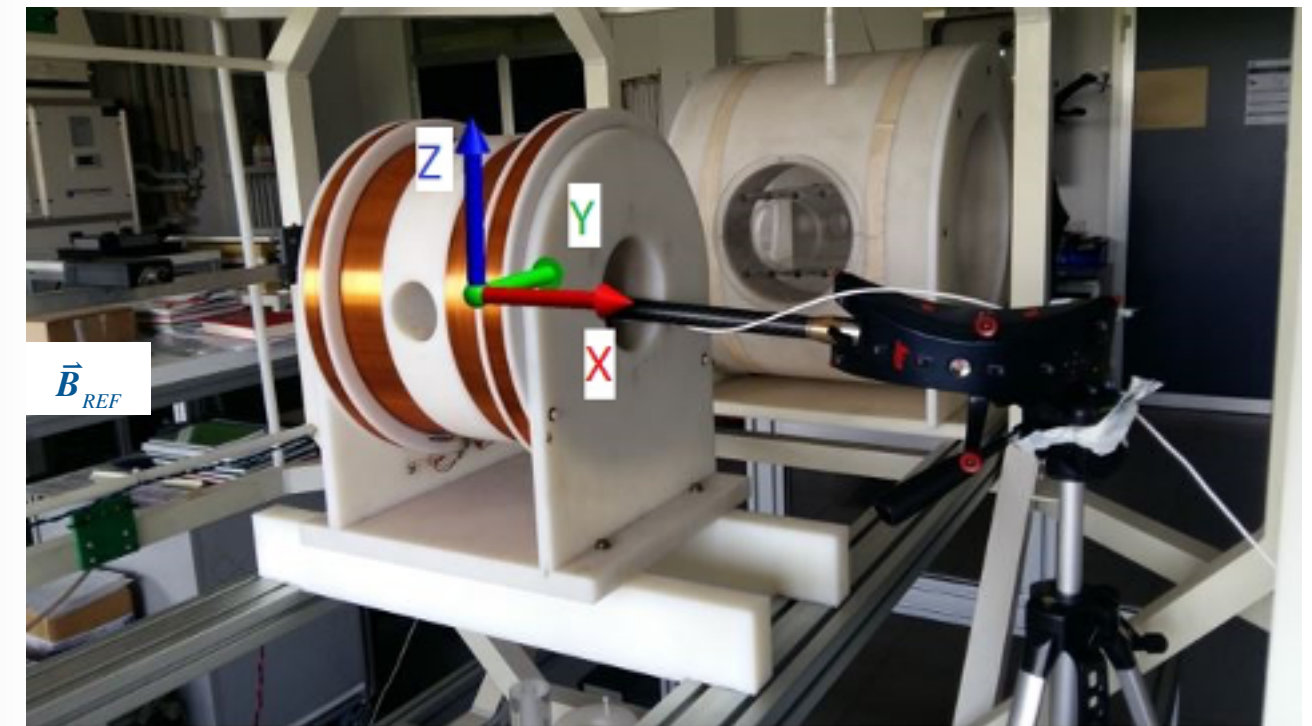

Figure 6. Calibration and uncertainty evaluation using a certified HH Coil @ INRIM.

The target function of the optimization is $J(\underline{C})$, defined as follows:

$$J\,(\underline{C},\ \vec{B}_{REF}\,) = \sum_i \| \vec{B}_{REF} - \underline{R}_i \cdot \underline{C} \cdot \vec{B}_{Hi} \|$$

The optimization parameters are the components of matrix $\underline{C}$ and the 2 Euler angles of the reference field β_x, β_z, that, in principle, are not known a-priori with enough precision.

The geometrical centre of the HH coil is detected probing the surface of the coils. High accuracy is not necessary, as the homogeneity volume is big enough to allow some errors in the evaluation of its centre.

Anyway, the optimization process produces an orientation of the reference field $\vec{B}_{REF}$ that differs from the geometrical approximation by 14.7 $mrad$ and β_z and 0.5 $mrad$ for β_z only. Nevertheless, the magnitude of these angles does not influence in any way the calibration procedure, as the reference field is fixed and uniform regardless of its orientation. Anyway, they give a good grasp of the quality of the geometrical characterization of the HH coil.

A campaign of 90 different measurements, with different combinations of current applied to the coils and orientation of the probe, was performed. The set of positions was chosen in order to have the minimum condition number for the system to be solved, i.e. to have enough orientation to maximize the sensitivity for each axis of the hall probe.

Mathematically speaking it is an over-constrained non-linear system of 90 equations with 8 unknowns to be solved via an iterative approach. The distribution of the relative error with respect to the reference field

$$\varepsilon\% = \frac{\| \vec{B}_{REF} - \vec{B}_{MEASi} \|}{\vec{B}_{REF}}\ \%\quad \text{is shown in Figure 7.}$$

The average is found to be 0.13% with a standard deviation of 0.05%. These numbers include also the uncertainty on $\vec{B}_{Hi}$ and on $\underline{R}_i$ produced by the Teslameter and by the Laser Tracker respectively.
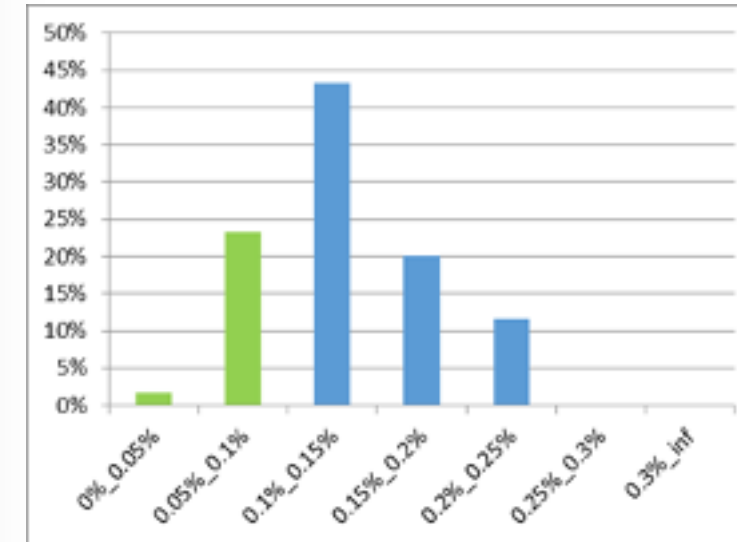

Figure 7. Distribution of relative error $\varepsilon\%$ of the measures after application of the calibration matrix.

A model for the uncertainty is calculated as follows:

$$U_{B_{Ai}} \approx \sqrt{(U_{B_{Hi}})^2 + (B_{Hi}\,U_{C_{ij}})^2}$$

Where U_i is the uncertainty on the *i-th* quantity.
The final uncertainty of the complete system is evaluated to be

$U_{C_{ij}} \approx 0.23\%$ @2σ for any measure performed in the applicable range of the campaign. $U_{B_{Hi}} = 7\mu T$.

A similar HH coil, characterized by 4 fiducials, was lately developed in order to perform in-house calibration in any moment.

Figure 8. A similar HH coil developed to perform the calibration procedure in house.

Magnetic field range	1mT - 20mT; Short time 50mT
Maximal current (for 20mT)	1.4A
Helmholtz Coil constant k = B/I [mT/ A]	14.353 mT/A
Non-linearity error in the applicable range (after 30')	1e-5
$\Delta H/H$ in 20mm sphere	< 4e-4
$\Delta H/H$ in 2mm sphere	< 4e-5
Resistance (series connected coils)	63 Ω
Turns	2 x 2200 x
Wire diameter	Ø1mm
Max power	125W

3. Examples of measured magnetic field

A tool is developed in .net Framework to coordinate the measurements of the Laser Tracker and the Teslameter all within a SpatialAnalyzer® (SA) environment. The software can instantly visualize the vector of the magnetic flux density inside the 3D environment of SA aligned to the CAD model of the object under inspection.

The tool was initially implemented to be flexible enough to measure a vector $\vec{B}$ in any visible and accessible position. For the present purpose some additional features were developed to streamline the process of acquisition and facilitate the sequence of actions to be performed by the operator (e.g. switch on/off the power supply of 200A DC or measure control points).

Depending on the measurements accuracy, the procedure might need a physical tool to precisely move the T-probe and keep it in a steady position for each single acquisition. If minor accuracy is acceptable, the T-probe could be moved by hand and the acquisition process might be significantly faster.
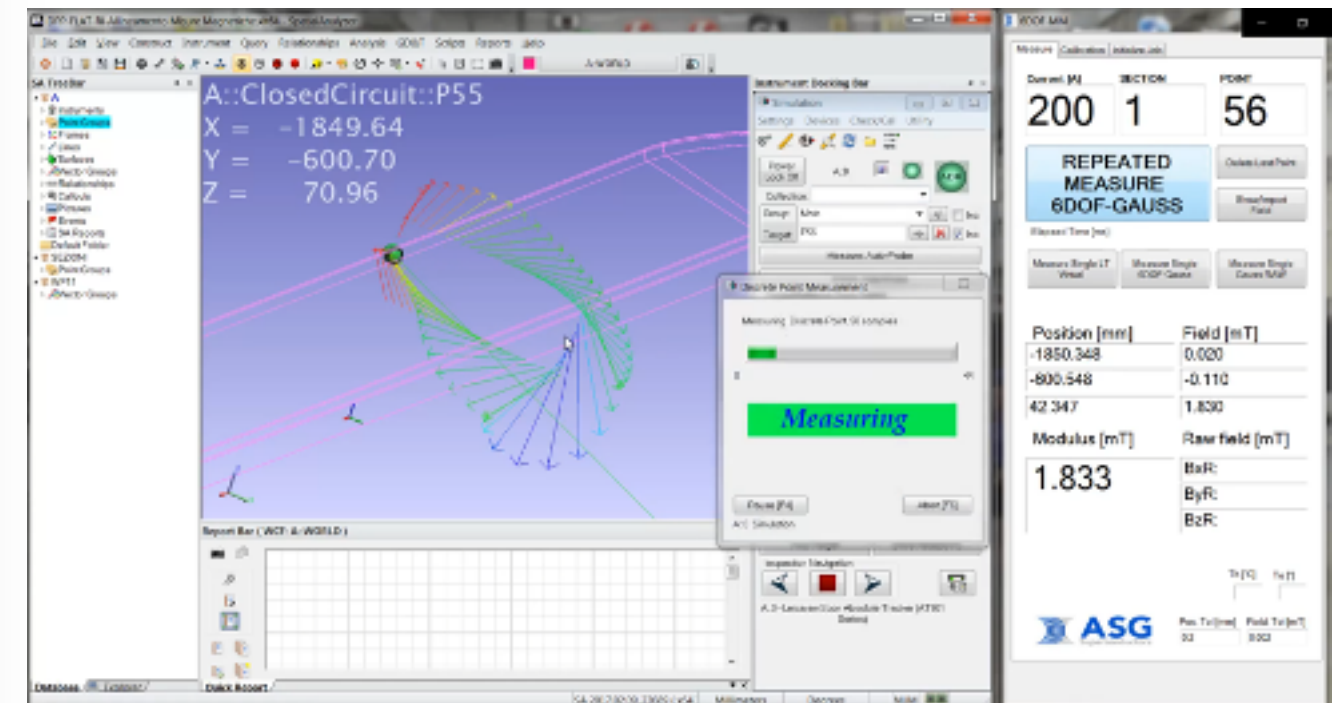

Figure 9. Snapshot of the GUI to control the 6DOF-MM device within SA.

A preliminary test was performed on the Double Pancake Prototype (DPP) coil. The line integral of the magnetic field around a closed loop was measured ($\Gamma(\vec{B})$) and calculated from theory (Γ_{CALC}). The relative difference was found to be only 0.14% despite the coarse grid used for the numerical approximation of the integral.

$$\Gamma(\vec{B}) := \oint \vec{B} \cdot d\vec{l} = \oint \vec{B} \cdot d\vec{l} \approx \frac{1}{2} \sum_i (\vec{B}_i + \vec{B}_{i+1}) \cdot (\vec{r}_{i+1} - \vec{r}_i) = -4530.2 \ mT \cdot mm$$

$$\Gamma_{CALC} = \mu_0 \sum_i I_i = -4\pi \cdot 10^{-7} \cdot 12 \cdot 300 \ T \cdot m = -4523.9 \ mT \cdot mm$$

$$\varepsilon_r = \frac{\Gamma(\vec{B}) - \Gamma_{CALC}}{\Gamma_{CALC}} \% = 0.14\%$$
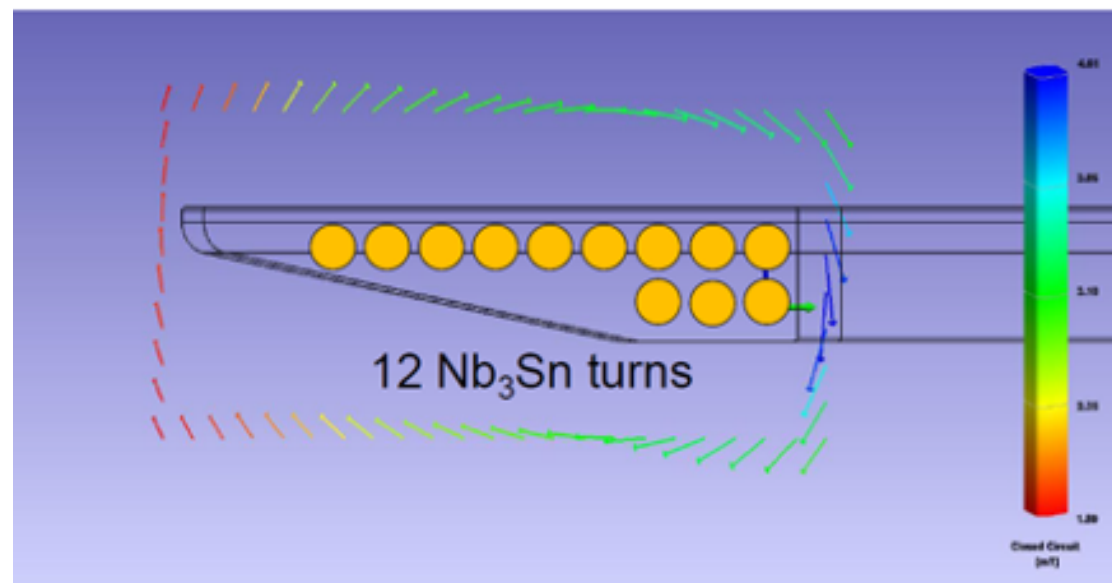
Figure 10. Line integral measure around a section of Double Pancake Prototype (DPP).

Measures on the WPs cannot be performed at nominal current of 68kA due to physical constraints. Therefore, a steady DC current of 200A is applied to the winding. The higher the current, the lower the noise to signal ratio. So, in principle, the current should be maximized. Pre-existent studies and practical tests had shown that, to avoid significant deformations due to thermal expansion, it is necessary to keep an unsteady current throughout the duration of the whole survey. The complete set of measurements could take up to 40 non-consecutive hours, therefore waiting for the thermal stabilization of the system is not worth the effort. For this reason, the current is switched on and off at each measuring section in order to minimize the thermal drift and avoid temperature compensations. Current stabilization is long enough to neglect any contribution from eddy currents.

All the ten Toroidal Field Winding Packs manufactured in ASG were measured with the described technique. Some snapshots of the WPs measured in 2017 are shown in the following pictures.

Figure 11. View of a WP inside the dedicated a-magnetic clean area at ASG premises (La Spezia). White tape visible on the coated surface was used to visualize the location of the sections to be measured and simplify the preliminary alignment of the device.
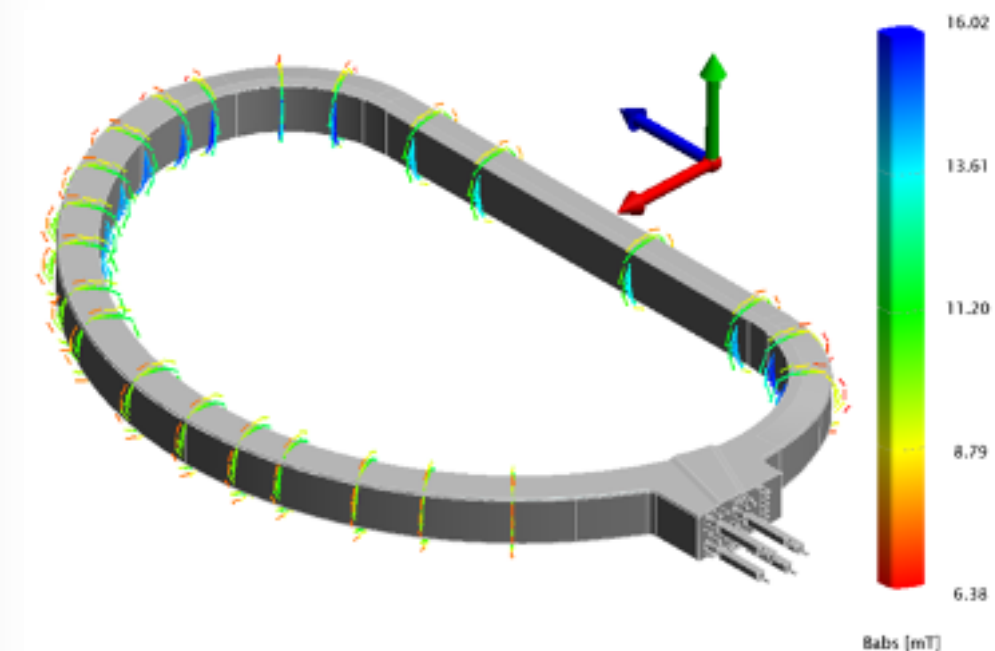

Figure 12. View of the entire WP magnetic flux density field at reduced current (200A) after numerical removal of the geomagnetic stray field. Vectors are proportional to the intensity |B| and are represented in the TGCS frame.
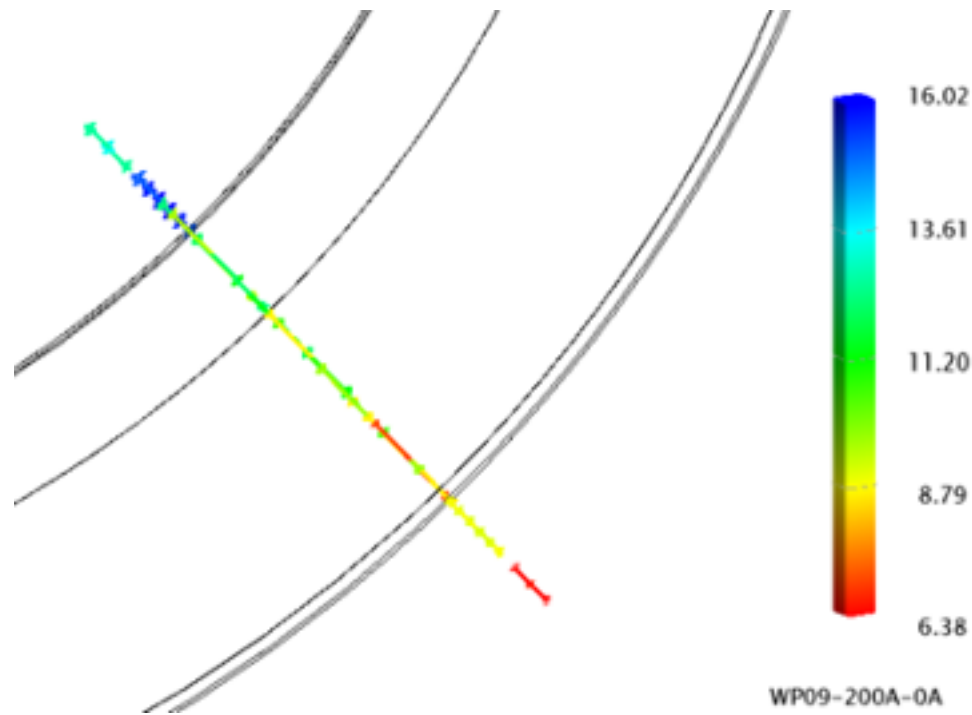
Figure 13. View of the magnetic field at reduced current (200A) after numerical removal of the stray field of a single section.
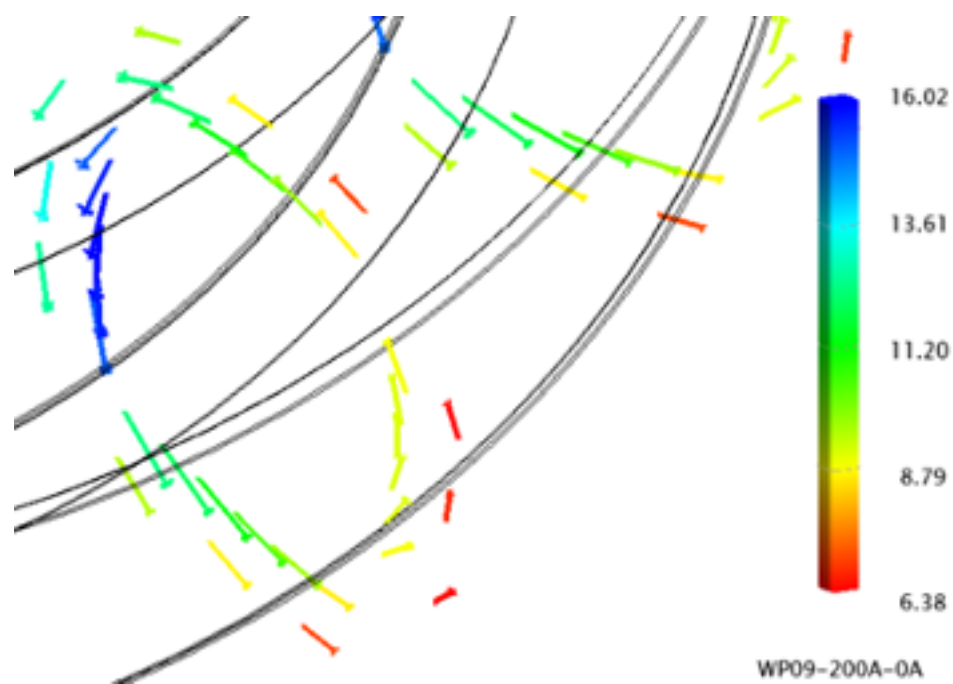

Figure 14. View of the magnetic field at reduced current (200A) after numerical removal of the stray field of the section in Figure 12.

4. Measurement statistics on 6 WPs

In the following pages, some statistic elements of the vector fields measured on 6 manufactured WPs are illustrated.

Definition: **Standard deviation σ** of the vector field of WPs at acquisition point "i"

$$\sigma_i = \sqrt{\frac{1}{N-1} \sum_{WP} \left(\vec{B}_{WPxi} - \left\langle \vec{B}_{WPxi} \right\rangle_{WP} \right)^2} \cdot 100\% \qquad \text{for } WP = 1, ..,6$$

Definition: **Magnetic Field Relative Difference** between WPx and average vector field of WPs at acquisition point "i"

$$\frac{dB_{WPi}}{B} = \frac{\| \vec{B}_{WPx} - \left\langle \vec{B}_{WPx} \right\rangle_i \|}{\| \left\langle \vec{B}_{WPx} \right\rangle_i \|} \cdot 100\%$$

Definition: **Geometrical Mean Deviation from Average**

$$\left\langle ds \right\rangle_{WP} = \left\| \left\langle \vec{dr}_{WPx} - \left\langle \vec{dr}_{WPx} \right\rangle_{WP} \right\rangle_i \right\|$$
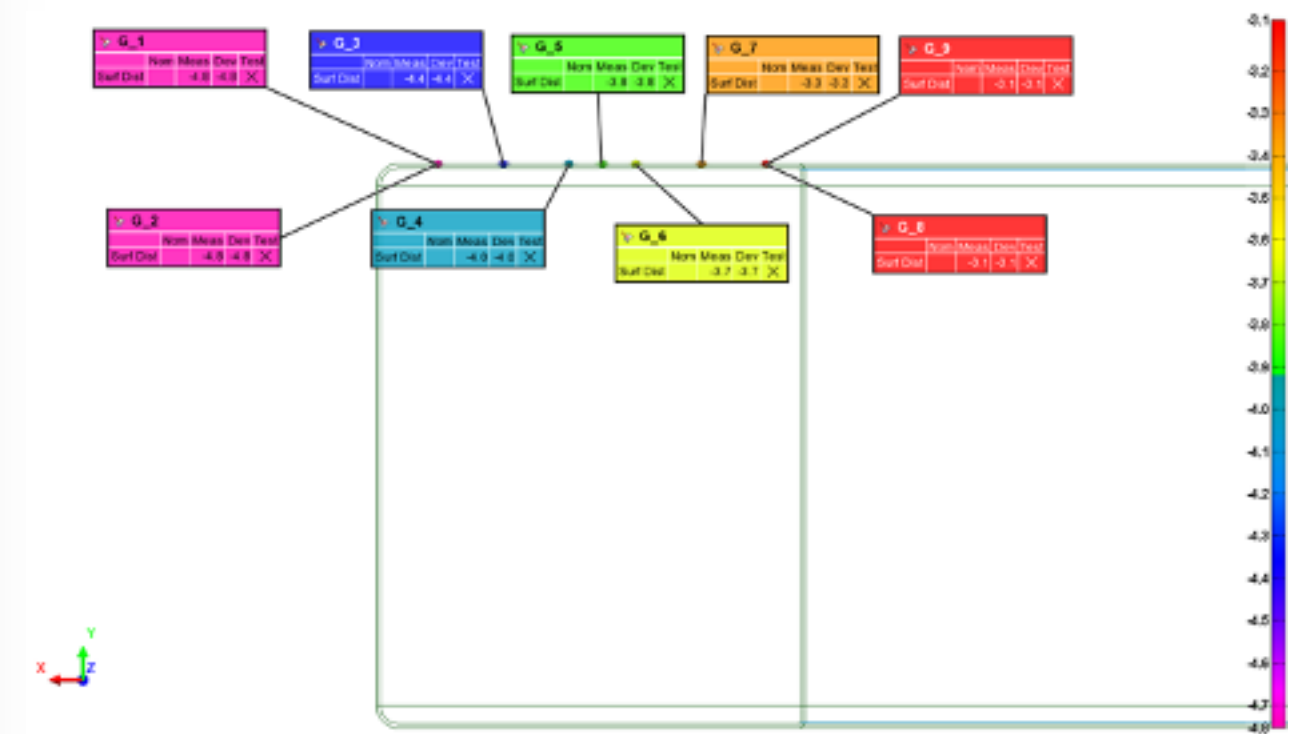

Figure 15. Deviation of the measured geometric surface from the nominal in correspondence to the projection of the measured magnetic points on the WP.
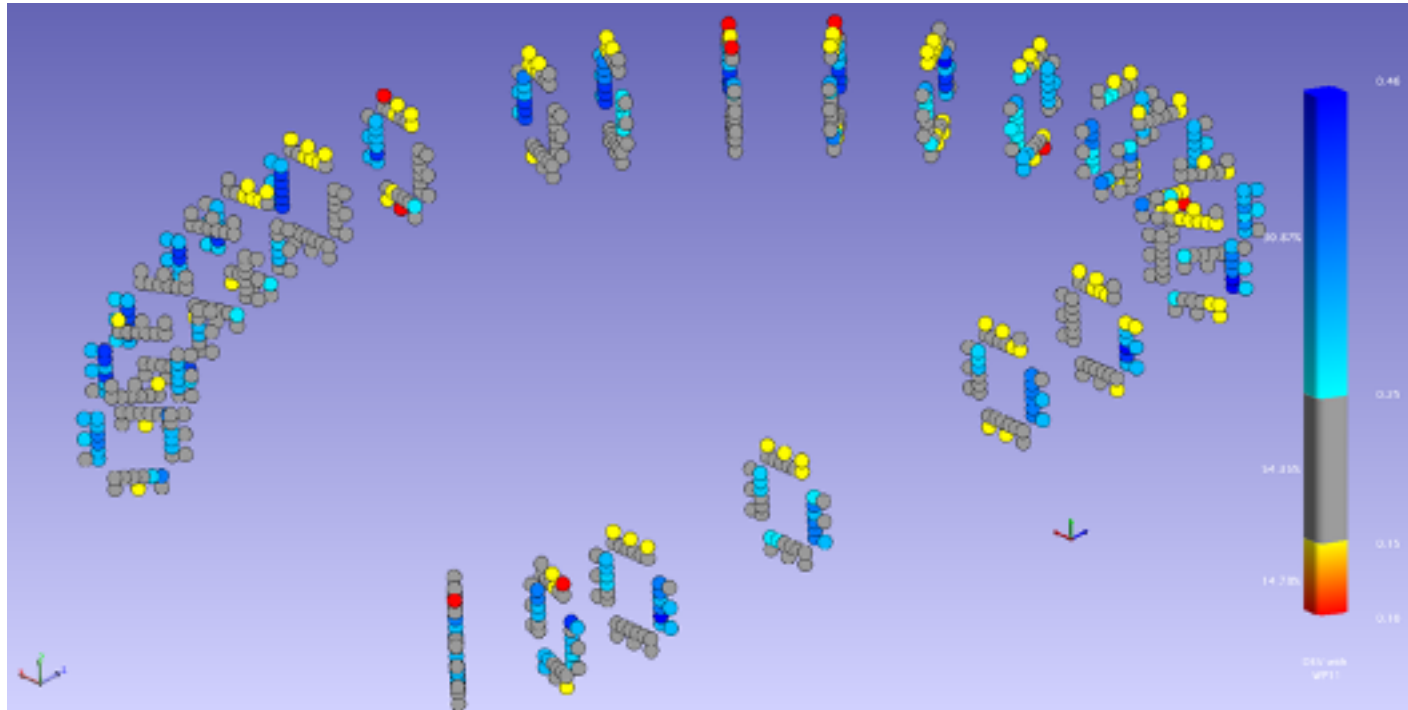
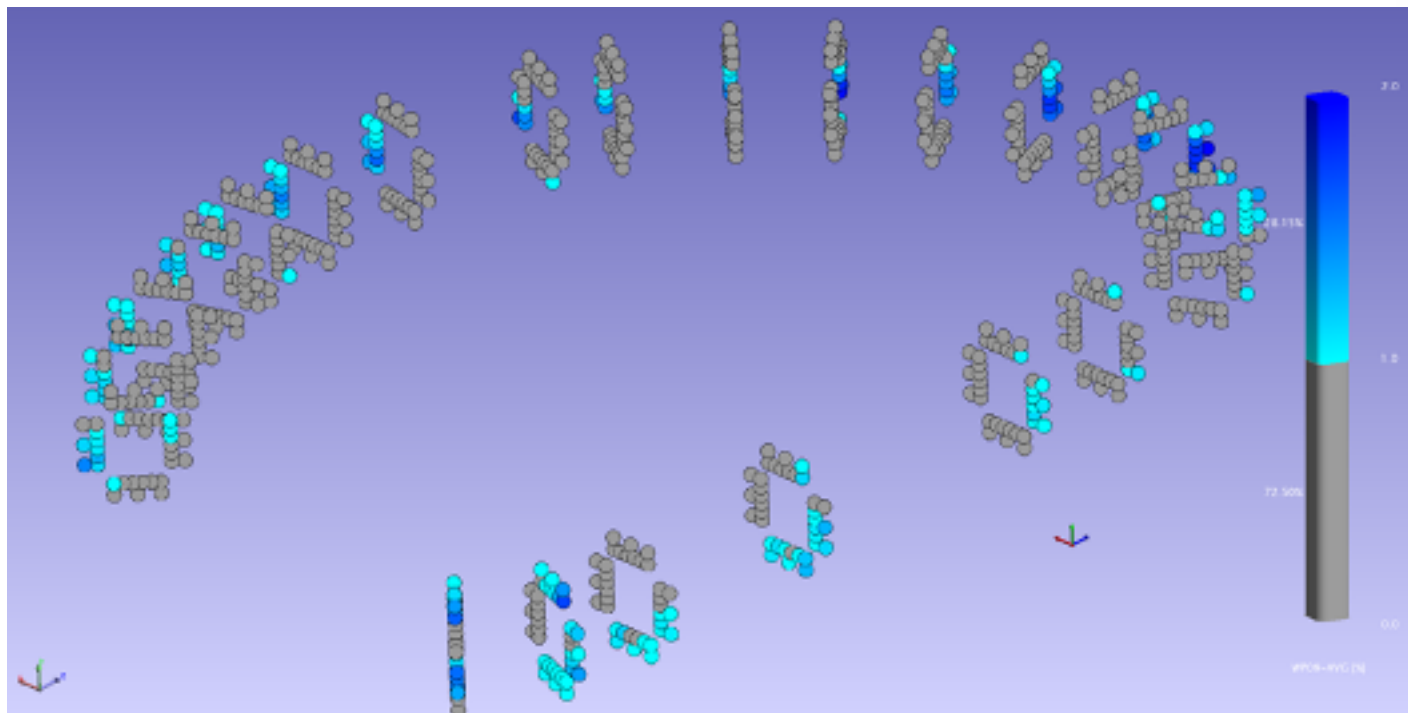**Figure 16**. Standard deviation σ of 6 vector field of 6 different WPs [mT].

Figure 17. Relative difference dB/B between WP09 and average.

In Figure 18 it is possible to appreciate the consistency of the geometrical manufacturing (horizontal axis) with respect to the consistency of the resulting magnetic field at reduced current (vertical axis).

Consistency of manufacturing is crucial to maximize the quality of the magnetic field generated by the Tokamak[6]. The more similar the WPs the higher the quality of the field.
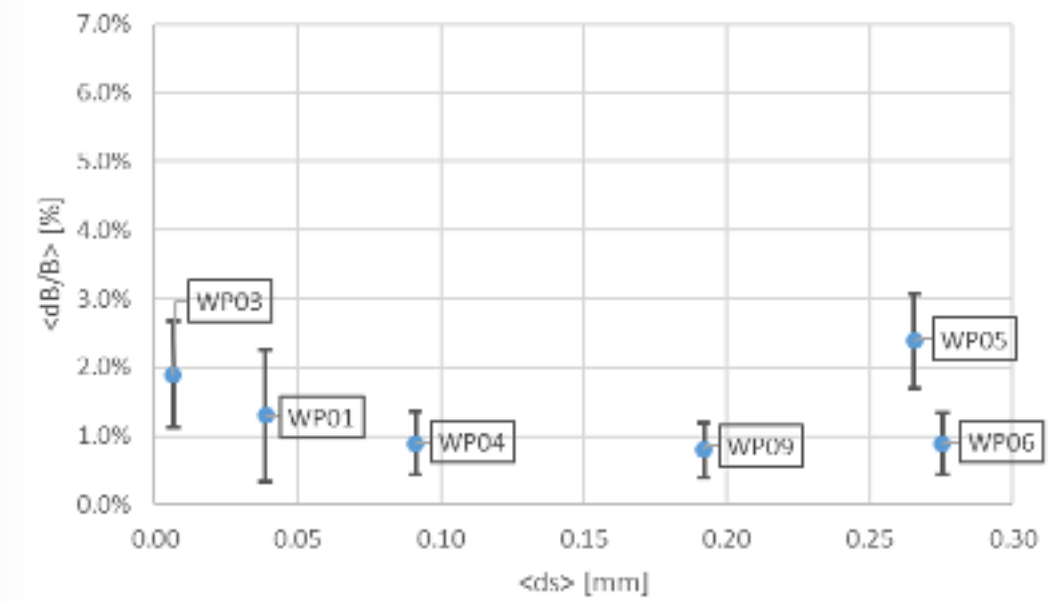
[6] N. Mitchell and J. Knaster: "Contribution to Plasma Error Fields from the CS, PF and TF coils", ITER_D_23DVQU, v. 1.3: 2 September 2006.

Figure 18. "Average Magnetic Field Relative Difference" <dB/B> plotted against the Geometrical Mean Deviation from Average ⟨ds⟩. Black error bars shows the standard deviation of the "Magnetic Field Relative Difference per each WP"